AUTHOR QUERY FORM

ELSEVIER	**Journal: GCA** **Article Number: 8649**	**Please e-mail or fax your responses and any corrections to:** **E-mail:** corrections.essd@elsevier.sps.co.in **Fax: +31 2048 52799**

Dear Author,

Please check your proof carefully and mark all corrections at the appropriate place in the proof (e.g., by using on-screen annotation in the PDF file) or compile them in a separate list. Note: if you opt to annotate the file with software other than Adobe Reader then please also highlight the appropriate place in the PDF file. To ensure fast publication of your paper please return your corrections within 48 hours.

For correction or revision of any artwork, please consult http://www.elsevier.com/artworkinstructions.

Any queries or remarks that have arisen during the processing of your manuscript are listed below and highlighted by flags in the proof. Click on the 'Q' link to go to the location in the proof.

Location in article	**Query / Remark:** click on the Q link to go **Please insert your reply or correction at the corresponding line in the proof**
Q1	Please confirm that given name(s) and surname(s) have been identified correctly.
Q2	The citation Smith (1999) has been changed as Smith et al. (1999) to match the author name in the reference list. Please check here and in subsequent occurrences, and correct if necessary.
Q3	Ref. Sun and Torgersen (1998)__ is cited in the text but not provided in the reference list. Please provide it in the reference list or delete these citations from the text.
Q4	In the sentence 'Terrestrial groundwater trace element and…', citation 'Section 4.3.3' is given, but no section 4.3.3 given in this article. Please check this occurrence.
Q5	Please note that Fig. 9 was not cited in the text. Please check that the citation is in the appropriate place, and correct if necessary.

Please check this box if you have no corrections to make to the PDF file ☐

Thank you for your assistance.

Highlights

• Chemical cycling of Ba, Sr, Ca, U, Mn and Ra within a karst subterranean estuary is evaluated. • Terrestrial groundwater reflects aquifer rock trace element content for Sr, Ca, Ba, Mn and Ra. • Ra and Ba chemical cycling is decoupled; both demonstrate low salinity desorption. • Spring mixing zone Ba, Sr, Ca and Mn cycling is largely conservative between terrestrial groundwater and the ocean. • Karst subterranean estuaries are a significant source of Ra, Sr and U to the ocean.

Available online at www.sciencedirect.com
ScienceDirect
Geochimica et Cosmochimica Acta xxx (2014) xxx–xxx
Geochimica et Cosmochimica Acta
www.elsevier.com/locate/gca

Trace element geochemistry of groundwater in a karst subterranean estuary (Yucatan Peninsula, Mexico)

Meagan Eagle Gonneea[a],*, Matthew A. Charette[a], Qian Liu[b], Jorge A. Herrera-Silveira[c], Sara M. Morales-Ojeda[c]

[a] *Department of Marine Chemistry and Geochemistry, Woods Hole Oceanographic Institution, Woods Hole, MA, USA*
[b] *State Key Laboratory of Marine Environmental Science, Xiamen University, Xiamen, China*
[c] *CINVESTAV-IPN, Unidad Mérida, A.P. 73 CORDEMEX, Mérida, Yucatán, Mexico*

Received 7 August 2013; accepted in revised form 28 January 2014; available online xxxx

Abstract

Trace element cycling within subterranean estuaries frequently alters the chemical signature of groundwater and may ultimately control the total chemical load to the coastal ocean associated with submarine groundwater discharge. Globally, karst landscapes occur over 12% of all coastlines. Subterranean estuaries in these regions are highly permeable, resulting in rapid infiltration of precipitation and transport of groundwater to the coast, and the predominant carbonate minerals are readily soluble. We studied the chemical cycling of barium (Ba), strontium (Sr), manganese (Mn), uranium (U), calcium (Ca) and radium (Ra) within the carbonate karst subterranean estuary of the Yucatan Peninsula, which is characterized by a terrestrial groundwater lens overlying marine groundwater intrusion with active submarine discharge through coastal springs. Terrestrial groundwater calcium (1–5 mmol kg^{-1}) and alkalinity (3–8 mmol kg^{-1}) are enriched over that predicted by equilibrium between recharging precipitation and calcite, which can be accounted for by groundwater organic matter respiration and subsequent dissolution of calcite, dolomite and gypsum. There is a close agreement between the observed terrestrial groundwater Sr/Ca, Mn/Ca, Ba/Ca and Ra/Ca and that predicted by equilibrium dissolution of calcite, thus the trace element content of terrestrial groundwater is largely determined by mineral dissolution. Subsequent mixing between terrestrial groundwater and the ocean within the actively discharging springs is characterized by conservative mixing of Sr, Mn, Ba and Ca, while U is variable and Ra displays a large enrichment (salinity: 1.9–34.9, Ba: 60–300 nmol kg^{-1}, Sr: 15–110 µmol kg^{-1}, U: 0.3–35 nmol kg^{-1}, Mn: 0.3–200 nmol kg^{-1}, Ca: 4.3–12.9 mmol kg^{-1}, ^{226}Ra: 18–2140 dpm 100 L^{-1}). The deep groundwater sampled through cenotes, local dissolution features, is typified by elevated Ba, Sr, Ca, Mn and Ra and the absence of U within marine groundwater, due to enhanced dissolution of the aquifer matrix following organic matter degradation and redox processes including sulfate reduction (salinity: 0.2–36.6, Ba: 7–1630 nmol kg^{-1}, Sr: 1.3–210 µmol kg^{-1}, U: 0.3–18 nmol kg^{-1}, Mn: 0.6–2600 nmol kg^{-1}, Ca: 2.1–15.2 mmol kg^{-1}, ^{226}Ra 20–5120 dpm 100 L^{-1}). However, there is no evidence in the spring geochemistry that deep marine groundwater within this reaction zone exchanges with the coastal ocean via spring discharge. Total submarine groundwater discharge rates calculated from radium tracers are 40–95 m^3 m^{-1} d^{-1}, with terrestrial discharge contributing 75 ± 25% of the total. Global estimates of chemical loading from karst subterranean estuaries suggest Sr and U fluxes are potentially 15–28% and 7–33% of total ocean inputs (8.2–15.3 mol y^{-1} and 4.0–7.7 mol y^{-1}), respectively. Radium-226 inputs from karst subterranean estuaries are 34–50 times river inputs (6.7–9.9 × 10^{16} dpm y^{-1}).

Abbreviations: *SGD, submarine groundwater discharge; STE, subterranean estuary; SI, saturation index.*

* Corresponding author. Tel.: +1 508 289 3236.

E-mail addresses: mgonneea@whoi.edu (M.E. Gonneea), mcharette@whoi.edu (M.A. Charette), qianqianliu@xmu.edu.cn (Q. Liu), jherrera@mda.cinvestav.mx (J.A. Herrera-Silveira), moojsa@gmail.com (S.M. Morales-Ojeda).

0016-7037/$ - see front matter © 2014 Published by Elsevier Ltd.
http://dx.doi.org/10.1016/j.gca.2014.01.037

Please cite this article in press as: Gonneea M. E., et al. Trace element geochemistry of groundwater in a karst subterranean estuary (Yucatan Peninsula, Mexico). *Geochim. Cosmochim. Acta* (2014), http://dx.doi.org/10.1016/j.gca.2014.01.037

1. INTRODUCTION

Submarine groundwater discharge (SGD) is the transport of terrestrially sourced groundwater and groundwater of marine origin across the ocean-aquifer interface (Burnett et al., 2006). Many studies have shown that SGD is an important source of trace elements to the coastal ocean (Shaw et al., 1998; Basu et al., 2001; Moore et al., 2006; Beck et al., 2007; Bone et al., 2007; Moore, 2010; Santos et al., 2011; Beck et al., 2013; Gonneea et al., 2013). However, uncertainty remains concerning the total chemical flux via SGD, due in part to groundwater transit through the subterranean estuary (STE), the region of the coastal aquifer where sharp gradients in salinity, oxygen and redox state facilitate the biogeochemical cycling of trace elements (Moore, 1999; Charette and Sholkovitz, 2006; Kaleris, 2006; Beck et al., 2007; Gonneea et al., 2008; Santos et al., 2011). To fully understand the impact SGD has on the coastal ocean and the role SGD plays in global ocean element budgets, we need to quantify how chemical cycling within the subterranean estuary impacts transport of dissolved species to the ocean.

Geochemical transformations within the salinity-mixing zone of the subterranean estuary have been observed at many sites characterized by permeable sand and dominated by aluminosilicate minerals (Charette and Sholkovitz, 2006; Beck et al., 2007; Gonneea et al., 2008; Santos et al., 2011). Karst subterranean estuaries, however, have three unique characteristics: (1) the water to rock ratio is much higher and more variable due to multiple scales of permeability; (2) carbonate minerals are readily soluble; and (3) groundwater mixing occurs during channelized conduit flow of both terrestrial and marine groundwater, with springs being the primary route of water exchange with the coastal ocean (Perry et al., 2002; Beddows et al., 2007; Fleury et al., 2007; Charette et al., 2008; Garcia-Solsona et al., 2010; Einsiedl, 2012). The key processes that may alter dissolved trace element distributions in the subterranean estuary include mineral dissolution/precipitation, adsorption/desorption reactions, redox cycling, and mixing between water sources. In the case of radioactive trace elements such as the isotopes of radium, radioactive production or decay must also be considered.

Globally, 12% of submarine groundwater discharge flows through karst subterranean estuaries (as reported in Beck et al. (2013) calculated from aquifer lithologies presented in Gibbs and Kump (1994) and regional SGD estimates in Zekster et al. (2006)). This study evaluates geochemical cycling of barium (Ba), uranium (U), strontium (Sr), manganese (Mn), calcium (Ca) and radium (^{226}Ra, ^{228}Ra and ^{223}Ra) within the Yucatan Peninsula karst subterranean estuary. These elements are of interest given their utility as tracers of environmental processes. For example, past oceanic productivity can be reconstructed from $BaSO_4$ burial rates (Paytan et al., 1996) while the oceanic Sr isotope record serves as a proxy for various inputs to the ocean, including continental weathering and hydrothermal circulation (Hess et al., 1986; Palmer and Edmond, 1989). Variability in oceanic Ca may be related to changes in ocean carbon cycling on long time scales (Griffith et al., 2008). Ra is used extensively as a tracer of groundwater discharge (Moore, 1996). Uranium serves as a proxy of ocean redox state (Tribovillard et al., 2006). More recently, studies have shown SGD associated fluxes and chemical transformations within the subterranean estuary should be considered in oceanic element budgets (Dunk et al., 2002; Santos et al., 2011; Holmden et al., 2012; Beck et al., 2013). To this end, SGD-derived chemical fluxes are determined for the Yucatan Peninsula. We then extrapolate the karst end members reported here to calculate potential global SGD derived chemical fluxes through karst subterranean estuaries and compare them to ocean element budgets.

2. METHODS

2.1. Field site

The Yucatan Peninsula is a large karst platform (165,000 km^2) that is bordered by the Gulf of Mexico along the west and north coasts and by the Caribbean Sea on the east coast (Fig. 1). The peninsula is characterized by a humid tropical climate, with maximum daily temperatures ranging from 25 to 35 °C and average rainfall that varies spatially across the Peninsula from 555 to –1500 mm y^{-1}. Evapotranspiration rates are ∼80% of total precipitation and invariant over the course of the year due to a low seasonal temperature difference and sustained vegetation growth (Bautista et al., 2009). The rainy season is from June through October with dry conditions prevailing from December through May, coinciding with cool temperatures (Giddings and Soto, 2003). From November through February temperatures are typically cool and north winds prevail. Tropical depressions, which frequently make landfall on the Yucatan Peninsula, result in large precipitation events (Boose, 2006).

The Yucatan Peninsula consists of limestone, dolomite and evaporite deposits, which can reach up to 1,500 m thickness (Bauer-Gottwein et al., 2011). The permeability of the aquifer is so great that there are no streams or rivers. Preferential flow paths in the karst aquifer range in scale from large dissolution conduits (10–100's of meters) to smaller scale fractures (1–10 cm), thus aquifer permeability is largely scale dependent. The hydraulic gradient is very low (1–10 cm km^{-1}) and flow is generally perpendicular to the coast (Hanshaw and Back, 1980; Beddows et al., 2007; Gondwe et al., 2010). Marine groundwater lies beneath a freshwater lens across the entire northern Peninsula, with the depth to the saltwater interface increasing with hydraulic head elevation, as predicted by the Dupuit-–Ghyben-–Herzberg model. Close to the coast (<20 km), the halocline is at < 40 m and it is possible to sample both terrestrial and marine groundwater through sinkholes, which are locally known as "cenotes" (Perry et al., 2009; Bauer-Gottwein et al., 2011). The freshwater portion of cenotes is typically oxic, with reducing conditions developing in the saline portions due to reduction of organic matter and presumably longer water residence times than terrestrial groundwater (Cervantes-Martinez et al., 2002; Perry et al., 2002; Schmitter-Soto et al., 2002; Torres-Talamante et al., 2011). A region of high permeability exists along the perimeter of the Cretaceous asteroid impact crater; known as the 'Ring of Cenotes', it bisects the coast at the Celestun and Bocas de Dzilam Lagoons (Perry et al., 1995).

Please cite this article in press as: Gonneea M. E., et al. Trace element geochemistry of groundwater in a karst subterranean estuary (Yucatan Peninsula, Mexico). *Geochim. Cosmochim. Acta* (2014), http://dx.doi.org/10.1016/j.gca.2014.01.037

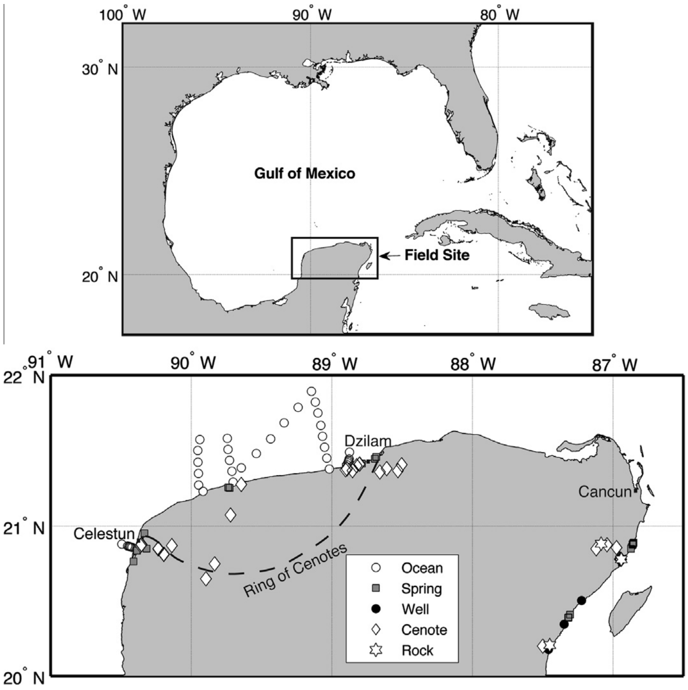

Fig. 1. Yucatan Peninsula field site. Samples were collected in 2007, 2009 and 2011, although not every site was sampled each year. The Ring of Cenotes is denoted in a dashed line between Celestun and Dzilam.

The degree of karstification of the Yucatan Peninsula results in high permeability with minimal surface flow (Perry et al., 2009; Bauer-Gottwein et al., 2011). Since the major vector for terrestrial freshwater transport to the coast is via SGD, many studies have evaluated its impact on the coastal ocean, with a particular focus on nutrient loading and eutrophication (Smith et al., 1999; Herrera-Silveira et al., 2002; ArandaCirerol et al., 2006; Young et al., 2008; Morales-Ojeda et al., 2010; Price et al., 2010). Seminal studies by Perry et al. (2002, 2009) have utilized groundwater major ion (i.e. Cl$^-$, Ca^{2+}, Mg^{2+}, K$^+$, Na$^+$, SO$_4^{2-}$) and strontium isotope chemistry to infer the subsurface geostratigraphy of the Yucatan Peninsula and groundwater flow paths across the region.

2.2. Field methods

Samples were collected during four field campaigns (May 26–29, 2007; December 4–9, 2009; February 12–17, 2011; and October 22–25, 2011) from cenotes, springs, wells and coastal ocean waters (Fig. 1). Springs were actively discharging into the coastal ocean and were either submerged or within the tidal zone. Well samples were collected only from the east coast and were pumped from 15 cm diameter wells with slotted casings extending down to 5–18 m. Ocean samples were collected within 60 km of the coast. Cenotes were sampled with a Niskin bottle in 2007 and a Proactive Mega-Typhoon™ submersible pump in 2009 and 2011. Cenote radium samples in 2007 were combined from multiple Niskin bottles and ranged from 3.4 to 10 L, while sample volume in 2009 and 2011 was 22–30 L. Spring samples were collected by placing a submersible pump within the outflowing water, with 4–30 L collected for radium. Coastal trace metal samples were collected from a Niskin bottle deployed at 2 m and radium samples (44–84 L) were collected from the same depth using a pump. Trace metal samples were passed through a 0.2 μm filter into clean LDPE bottles and acidified to pH 1 with Optima nitric acid. Dissolved inorganic carbon (DIC) and total alkalinity samples were passed through a 0.2 μm filter into 125 mL glass bottles, poisoned with 50 μL saturated mercuric chloride upon sample collection and were kept free of air bubbles. Samples for radium were filtered through MnO$_2$ impregnated acrylic fibers (hereafter referred to as Mn fibers) at a flow rate of 0.2–0.8 L min^{-1} to quantitatively sorb Ra onto the MnO$_2$ (Moore and Reid, 1973).

Basic water chemistry data including salinity, dissolved oxygen, temperature, pH and oxidation–reduction potential (ORP, converted to Eh) were measured in the field with a YSI 600XLM or a YSI 6920V2 multi-parameter sonde in a flow-through cell (springs and cenotes) or directly in the coastal ocean. In addition, separate water samples were collected in 2009 and 2011 for salinity and were analyzed by a Guideline AutoSal instrument. Three samples of the surficial aquifer rock were collected in 2009 from the east coast.

2.3. Analytical methods

Uranium, barium, and strontium were measured via isotope dilution on a 20 times diluted sample. Briefly, 0.075 g of sample was spiked with ^{135}Ba, ^{236}U and ^{84}Sr and diluted to 1.8 g with 5% Optima nitric acid. The resulting solution was analyzed on a Finnigan Element 2 high resolution inductively coupled plasma mass spectrometer (ICP-MS) at the Woods Hole Oceanographic Institution for masses ^{84}Sr, ^{88}Sr, ^{135}Ba, ^{138}Ba, ^{236}U and ^{238}U. The ^{84}Sr peak was

Please cite this article in press as: Gonneea M. E., et al. Trace element geochemistry of groundwater in a karst subterranean estuary (Yucatan Peninsula, Mexico). *Geochim. Cosmochim. Acta* (2014), http://dx.doi.org/10.1016/j.gca.2014.01.037

corrected for rubidium and krypton interferences. Manganese and calcium (for a subset of samples) were determined separately by diluting samples 20-fold with 5% Optima nitric acid and adding Indium (In) as an internal standard to account for instrument drift and matrix interferences of the solution. Count rates were normalized to In and concentrations were calculated from a standard curve. An additional subset of samples was run for Ca on a Dionex ion chromatograph. NASS-5, SLEW-3, SLRS-4 and IAPSO reference standards were run to determine accuracy, which was better than 1% for Ca, 5% for U, Sr and Ba, and 15% for Mn (Table S1). DIC and total alkalinity were measured within two weeks of collection. DIC was determined by acidification of 0.5 mL of a water sample and the subsequent quantification of CO_2 with a non-dispersive IR detector (Li-Cor 6252). The analytical precision is $\pm 3\ \mu mol\ kg^{-1}$. Total alkalinity was determined using Gran titration (Metrohm 808 Titrando with 1 mL burette) with precision of $\pm 4\ \mu mol\ kg^{-1}$. Both DIC and total alkalinity were calibrated by certified reference materials from A.G. Dickson of Scripps Institution of Oceanography. The aquifer rock samples were drilled to a fine powder, dissolved in 5% nitric acid and then trace elements were analyzed as described above.

The Mn fibers were rinsed with Ra-free water to remove salts, which interfere with counting (Sun and Torgersen, 1998), partially dried and placed within a delayed coincidence counter to measure ^{223}Ra and ^{224}Ra 1–6 days after collection (Moore and Arnold, 1996). For the oldest samples (6 days), only 30% of the initial ^{224}Ra remained. Samples from 2007 were counted at four weeks and two months post sampling to correct ^{223}Ra for ^{227}Ac adsorbed to the Mn fibers. In 2009 and 2011, an additional count was done at 11 to 17 days post sampling to improve ^{223}Ra measurements. Due primarily to low ^{224}Ra activities and decay during transit from Mexico, the majority of groundwater ^{224}Ra values were below detection and are not reported here[1]. Note that several water samples collected from deep cenotes for radium analysis were highly reducing, and despite aeration, the Ra could not effectively be removed from these samples due to loss of Mn oxide coating. Radium-223 activities of the surficial rock samples were determined by dissolving 20–30 g of powdered carbonate in 20% HCl, which was then neutralized to pH 8 with NaOH. Mn fibers were added to each solution and shaken for 24 h to remove radium. The Mn fibers were then rinsed and counted as above.

Manganese fibers were ashed (820 °C, 16 h), homogenized and capped with epoxy, prior to being placed within a well-type gamma spectrometer to measure ^{228}Ra (via ^{228}Ac at 911 keV) and ^{226}Ra (via ^{214}Pb at 351.9 keV) (Charette et al., 2001). All detectors were standardized using a ^{226}Ra NIST-certified Standard Reference Material (#4967A) and a gravimetrically prepared $ThNO_3$ powder, with Th daughters (^{228}Ra) in equilibrium, which was dissolved and calibrated via isotope dilution MC-ICP-MS with the ^{226}Ra NIST standard. These standard solutions were sorbed to Mn fibers and prepared in the same manner as the samples. Gamma counting detection limits (0.2 dpm) were calculated with the Currie Hypothesis test and were equivalent to 5 dpm 100 L^{-1} for 4 L cenote and spring samples and 0.2 dpm 100 L^{-1} for 84 L offshore samples (De Greer, 2004). ^{223}Ra and ^{228}Ra activities were decay corrected to the time of collection. Aquifer rock samples were drilled to a fine powder, capped with epoxy as above and ^{228}Ra and ^{226}Ra were quantified on gamma detectors.

2.4. Geochemical modeling

We used model simulations to determine how organic matter respiration could alter the groundwater chemistry through enhanced mineral dissolution. All groundwater speciation and mineral solubility calculations were performed with PHREEQ (Parkhurst and Appelo, 2013). The modeling was done with the Pitzer aqueous ion-interaction model using the PHREEQ reaction database. The actual composition of groundwater organic matter was not determined, so in our model we chose a simple organic substrate ($CH_2O(NH_3)$) to react at a fixed pressure of 1.1 atm. Organic matter (0.1–16 mmol kg^{-1}) was first reacted in the groundwater and then the modeled solution was allowed to equilibrate with three different mineral assemblages: (1) 100% calcite (1 mol L-1), (2) 95% calcite and 5% dolomite ($MgCa(CO_3)_2$) and (3) 95% calcite, 4.75% dolomite and 0.25% gypsum/anhydrite ($CaSO_4$/$CaSO_42(H_2O)$). Typical contributions of dolomite to the aquifer matrix are 5%; however, in regions of the aquifer where dolomitization has occurred, such as near the impact crater, it may be as much as 50% (Schmitt et al., 2004; Tuchscherer et al., 2005; Escobar-Sanchez and Urrutia-Fucugauchi, 2010). Since all of our groundwater samples are from the top 50 m of the aquifer, an upper limit dolomite to calcite ratio of 5% is used in the modeling here.

---

[1] The delayed coincidence counter employs a timed gate to differentiate between decay events associated with ^{224}Ra (^{224}Ra ($t_{1/2} = 3.6$ d)-^{220}Rn ($t_{1/2} = 55$ s)-^{216}Po ($t_{1/2} = 150$ ms)) and ^{223}Ra (^{223}Ra ($t_{1/2} = = 11.4$ d)-^{219}Rn ($t_{1/2} = 4.0$ s)-^{215}Po ($t_{1/2} = 1.78$ ms)), and records decay events associated with each isotope in two different channels on the detector (Moore and Arnold, 1996). However, some counts recorded in each channel are not associated with the targeted Ra isotope. These are known as chance coincidence events, and can be subtracted based on probability statistics (Giffin et al., 1963). Since the chance coincidence rate increases as the square of the total count rate of the system, ^{224}Ra and ^{223}Ra uncertainties increase at high total count rates and at very high total count rates, the chance coincidence corrections break down, particularly for ^{224}Ra (Moore and Arnold, 1996). This is observed in the detector counting logs as an increase in the chance coincidence corrected values over time. Thus, we evaluated the counting logs from every sample to ensure that there were no anomalous increases in either corrected ^{219}Rn (for measurement of ^{223}Ra) or ^{220}Rn (for measurement of ^{224}Ra). If the difference in the corrected cpm between the beginning and end of the counting period differed by more than 20%, that data was considered unreliable. We observed that many of the ^{224}Ra values in cenote and spring samples could not be measured with the RaDeCC system, likely due to high ^{223}Ra and ^{226}Ra activities in these samples. ^{224}Ra values are not reported since they were either below detection or unreliable due to the breakdown in chance coincidence calculations.

Please cite this article in press as: Gonneea M. E., et al. Trace element geochemistry of groundwater in a karst subterranean estuary (Yucatan Peninsula, Mexico). *Geochim. Cosmochim. Acta* (2014), http://dx.doi.org/10.1016/j.gca.2014.01.037

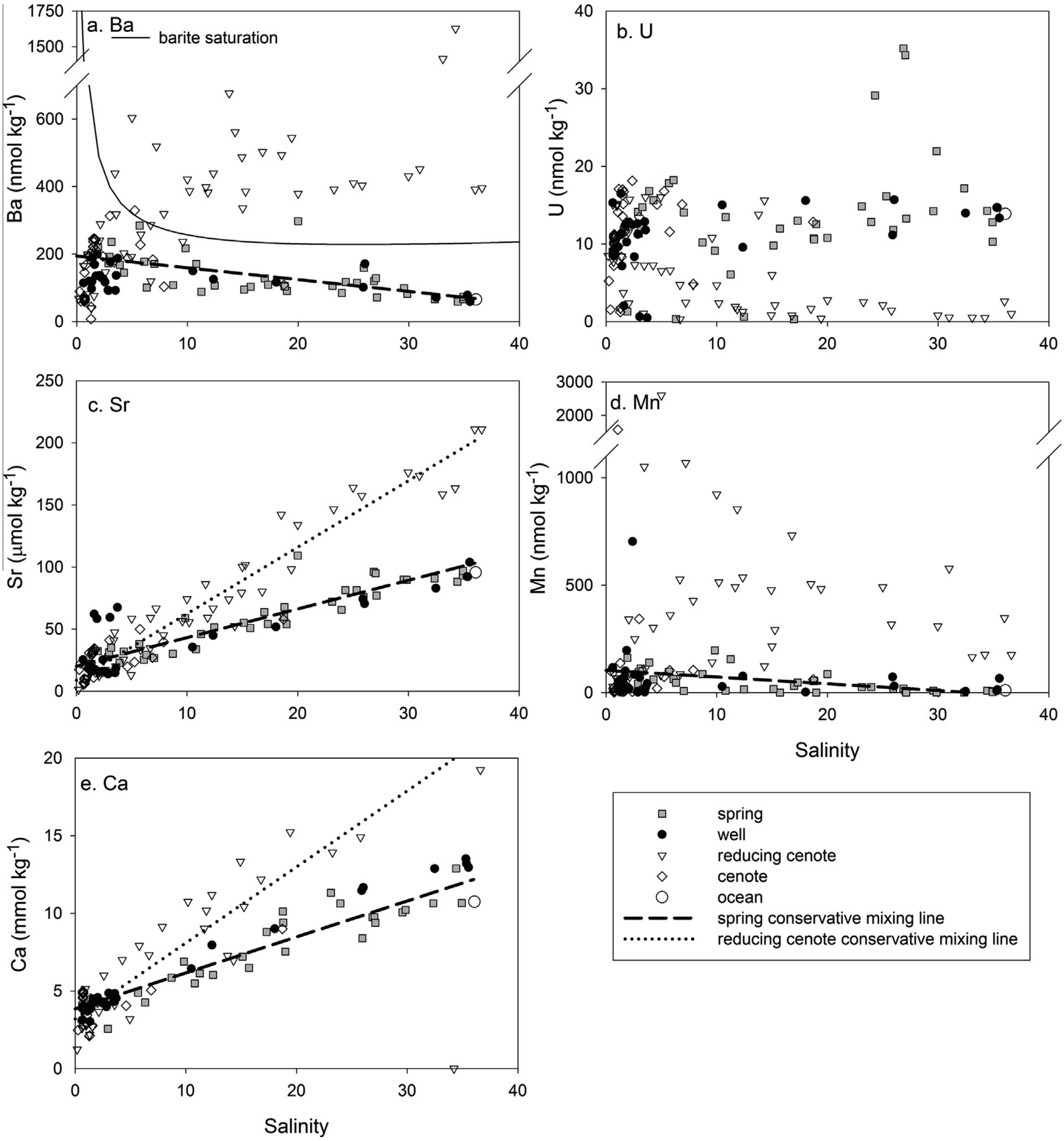

Fig. 2. Element plotted against salinity for (a) barium, (b) uranium, (c) strontium, (d) manganese, and (e) calcium. The barite solubility line is shown in (a) assuming a seawater sulfate end member of 28.2 mmol kg^{-1}. Statistically significant ($p < 0.0001$) conservative mixing lines for spring samples (dashed lines) and reducing cenote samples (dotted lines) are shown (Table S3). Spring samples were taken from actively discharging groundwater in the coastal ocean, well samples were pumped from shallow drilled wells near the coast, and cenote samples were collected from natural dissolution features. Note scale break in a and d.

3. RESULTS

3.1. Barium

Barium concentrations in cenote waters are elevated over ocean end members, with the highest concentrations found in reducing cenote waters (Eh < 200, 400–600 nmol kg^{-1}; Fig. 2a and Table S2); at depths >62 m in a cenote on the North coast (YT 175 and 176, Table S2), Ba values exceeded 1400 nmol kg^{-1}. In contrast, low salinity spring, well and cenote samples had lower, but very similar Ba concentrations (∼125 nmol kg^{-1}) with peak values observed at salinity ∼2. This type of non-conservative enrichment has been previously observed for Ba in subterranean estuaries (Shaw et al., 1998; Charette and Sholkovitz, 2006; Santos et al., 2011). Spring samples

Please cite this article in press as: Gonneea M. E., et al. Trace element geochemistry of groundwater in a karst subterranean estuary (Yucatan Peninsula, Mexico). *Geochim. Cosmochim. Acta* (2014), http://dx.doi.org/10.1016/j.gca.2014.01.037

(140 ± 60 nmol kg^{-1}) fall along a conservative mixing line between coastal ocean Ba values (65 ± 10 nmol kg^{-1}) and the salinity ~2 end member (dashed line in Fig. 2a, Table S3). In the reducing cenote waters, the high Ba concentrations would be supersaturated with respect to barite ($BaSO_4$) formation (Rushdi et al., 2000) if seawater SO_4^{2-} concentrations persisted, however, sulfate reduction and depletion has been detected in this region of the aquifer (Perry et al., 2002, 2009).

3.2. Uranium

Low salinity cenote waters range from 1.6 to 15.7 nmol kg^{-1} U, and low salinity spring and well samples typically have U concentrations >10 nmol kg^{-1} (Fig. 2b and Table S2). High salinity, reducing cenote samples are marked by depletion of U relative to predicted values for oxygenated seawater. Spring U concentrations are largely invariant across the salinity-mixing zone between terrestrial groundwater and the coastal ocean value (14 ± 0.5 nmol kg^{-1}).

3.3. Strontium

There are two conservative mixing relationships apparent in the strontium data (Fig. 2c and Table S2). Strontium concentrations range from 1 to 34 μmol kg^{-1} in low salinity spring, well and cenote samples although some well samples reach 50 μmol kg^{-1} at salinities 2–5. Reducing cenote samples then follow a conservative mixing line to peak values of 210 μmol kg^{-1} at salinity 36.6. Spring and well samples fall along a separate mixing line between a 20 μmol kg^{-1} low salinity end member and the coastal ocean (96 ± 3 μmol kg^{-1}) with the exception of a few low salinity well samples that are enriched in Sr (~60 μmol kg^{-1}). All samples are undersaturated with respect to celestite ($SrSO_4$), which reaches saturation at 450 μmol kg^{-1} Sr at salinity greater than 15, assuming conservative seawater SO_4^{2-} concentrations (Rushdi et al., 2000).

3.4. Manganese

Manganese concentrations are generally less than 100 nmol kg^{-1} in the low salinity cenote groundwater (Fig. 2d and Table S3). Higher salinity, reducing groundwater is comparatively enriched in manganese (10–2600 nmol kg^{-1}). Mixed salinity spring and coastal well samples mix conservatively between terrestrial groundwater (80 ± 160 nmol kg^{-1}) and coastal ocean (9.6 ± 4 nmol kg^{-1}) end members (Table S3).

3.5. Calcium

Calcium was only measured on a subset of the samples. Calcium is conservative with salinity, with two distinct mixing relationships (Fig. 2e and Table S2). Terrestrial groundwater is enriched in Ca (3.8 ± 0.9 mmol kg^{-1}) with spring samples falling on a mixing line (slope of 0.23 and intercept of 3.4) with the coastal ocean value (10.7 mmol kg^{-1}). Previously reported Ca values for Yucatan groundwater fall along a similar mixing line as the terrestrial groundwater and mixed salinity springs and wells (slope 0.19 and intercept 3.4 (Stoessell et al., 1989); slope 0.18 and intercept 4.2 (Reeve and Perry, 1994)). The mixing line for the deep reducing cenote samples from Sabtun Cenote shown here (slope of 0.59 and intercept of 3.7) intersects deep (UNAM2, 300 m) samples enriched in Ca reported in Perry et al. (2002), although the high Ca samples shown here are from a maximum depth of 35 m. Other reducing cenote samples are enriched in Ca to a lesser extent.

3.6. Radium isotopes

Radium-226 ($t_{1/2}$ = 1600 y) and ^{223}Ra ($t_{1/2}$ = 11.4 d) are enriched 100 and 230 times, respectively in groundwater compared to coastal ocean activities. Radium-228 ($t_{1/2}$ = 5.7 y) is comparatively less enriched (14 times) since its particle reactive parent (^{232}Th) occurs in very low abundance in both seawater and carbonate minerals (Fig. 3). This pattern is also observed in low salinity groundwater, from both cenotes and wells, which are approximately 20 times enriched in ^{226}Ra (360 ± 380 dpm 100 L^{-1}, Fig. 3a) and ^{223}Ra (21 ± 35 dpm 100 L^{-1}, Fig. 3c) compared to coastal ocean activities, while ^{228}Ra is only four times higher in low salinity groundwater (24 ± 20 dpm 100 L^{-1}, Fig. 3b) than in the coastal ocean. The two long-lived isotopes peak in spring samples at a salinity of ~5 (^{226}Ra: 2200 dpm 100 L^{-1}, ^{228}Ra: 180 dpm 100 L^{-1}), while the short-lived ^{223}Ra spring samples do not display a distinct peak (Fig. 3). Several high salinity cenote samples have very high ^{226}Ra (>3000 dpm 100 L^{-1}) and ^{228}Ra (>400 dpm 100 L^{-1}) without a corresponding enrichment of ^{223}Ra.

3.7. Aquifer rock trace elements and radium

The trace element content of the Yucatan surficial aquifer rock collected 10 km inland is: Ba = 0.17 μmol g^{-1}, Sr = 3.3 μmol g^{-1}, U = 3.2 nmol g^{-1}, Mn = 0.24 μmol g^{-1} (Table 1). Radium isotopes were also measured on two additional samples (collected 0.5 and 20 km from the coast) and displayed a large range: ^{228}Ra = 0.17–0.28 dpm g^{-1}, ^{226}Ra = 1.8–6.1 dpm g^{-1} and ^{223}Ra = 0.02–0.22 dpm g^{-1} (Table 1).

4. DISCUSSION

4.1. Aquifer rock geochemistry

The Ba, Sr, U and Mn content of the Yucatan aquifer rock reported here is slightly lower than global limestone values, likely due to some aluminosilicate inclusions in the global average limestone. The Yucatan carbonate aquifer we measured has minimal terrestrially-derived inclusions evidenced by a much lower Mn content, however there is a high silicate content due to the presence of diatom frustrules. Unaltered carbonate rocks from of the Chicxulub meteor impact zone (northwest Yucatan) have similar trace metal concentrations as those analyzed during this study (Table 1). Ba concentrations in unaltered carbonates

Please cite this article in press as: Gonneea M. E., et al. Trace element geochemistry of groundwater in a karst subterranean estuary (Yucatan Peninsula, Mexico). *Geochim. Cosmochim. Acta* (2014), http://dx.doi.org/10.1016/j.gca.2014.01.037

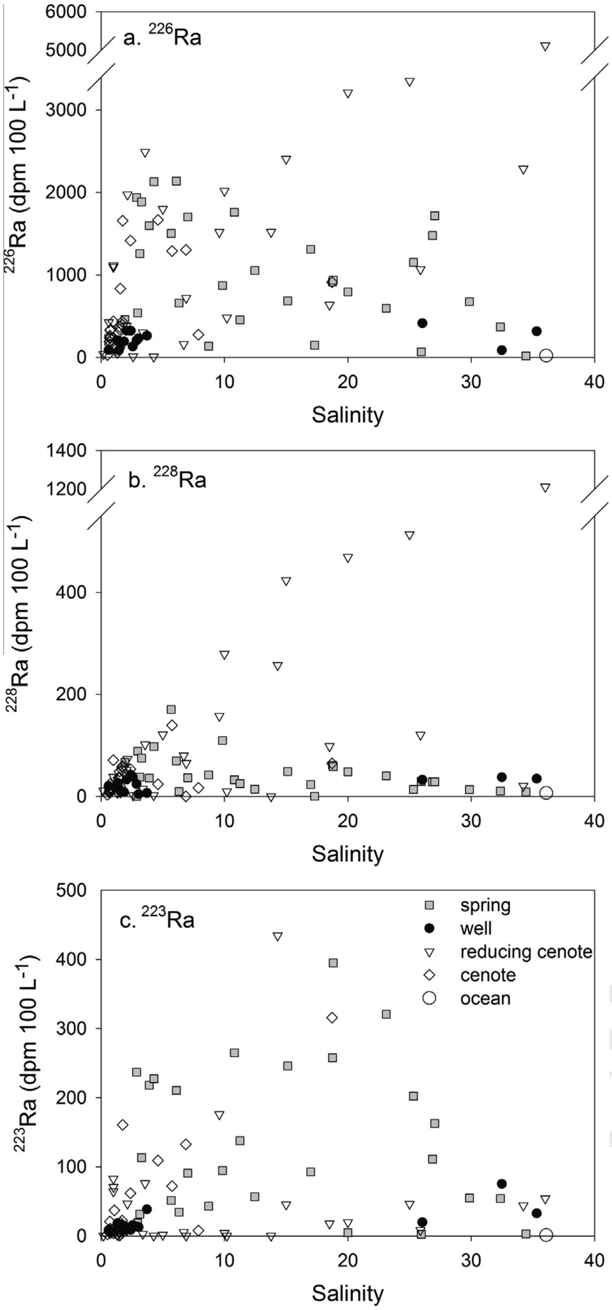

Fig. 3. (a) ^{226}Ra, (b) ^{228}Ra and (c) ^{223}Ra plotted against salinity. Note scale breaks in a and b.

ranged from 0.07–0.22 μmol g^{-1}, in close agreement with samples from the east coast (0.17 μmol g^{-1}, Table 1) (Tuchscherer et al., 2005). Sr content was slightly higher in the sample reported here (3.3 versus 2.3–2.6 μmol g^{-1}), while U and Mn are 30–40% lower in the sample analyzed here than near the impact zone. These differences may be potentially due to alteration associated with the bolide impact or subsequent changes in hydrogeology and weathering (Schmitt et al., 2004; Tuchscherer et al., 2005). There was a larger range in the sediment radium activities, particularly for ^{223}Ra and ^{226}Ra (within the ^{235}U and ^{238}U decay series respectively). The radium content of carbonate minerals is largely determined by the U present at the time of formation, leading to a large range in radium activities (Langmuir and Riese, 1985).

4.2. Geochemistry of the karst subterranean estuary terrestrial end member

Numerous studies of this aquifer have shown that groundwater is in equilibrium with calcite, the primary aquifer mineral (Stoessell et al., 1989; Reeve and Perry, 1994; Perry et al., 2002, 2009;). In addition, aragonite, celestite ($SrSO_4$) and evaporite layers (gypsum and anhydrite) occur in certain parts of the aquifer and dissolution of these minerals may further modify groundwater chemistry (Stoessell et al., 1989, 1993; Perry et al., 2002, 2009). Water in equilibrium with atmospheric CO_2 has a pH of 5.6; when this water reacts with calcite the resulting solution has a pH of 8.2, an alkalinity of 1100 μmol kg^{-1} and a dissolved Ca concentration of 0.5 mmol kg^{-1}. In contrast, our samples of Yucatan terrestrial (salinity < 2) groundwater had an alkalinity of 6460 ± 1210 μeq kg^{-1}, DIC of 6630 ± 1230 μmol kg^{-1}, pH of 7.25 ± 0.56 and 3.8 ± 0.9 mmol kg^{-1} dissolved Ca. To acquire this elevated alkalinity, DIC and Ca content, further mineral dissolution must be induced under elevated groundwater pCO_2 concentration and reduced pH. This modeling exercise is primarily meant to demonstrate the potential coupling between organic matter respiration and mineral dissolution that is necessary to explain the elevated dissolved Ca (and by proxy trace elements associated with $CaCO_3$) in terrestrial groundwaters and is not exhaustive due to the paucity of carbonate chemistry available for this data set. We compared the total dissolved calcium, alkalinity and DIC of the modeled groundwater to a subset of samples (collected in 2009) for which carbonate chemistry (i.e. alkalinity, dissolved inorganic carbon) was determined.

We reacted 0.1–16 mmol kg^{-1} organic matter and then allowed the resulting solution to reach equilibrium with calcite (1 mol L^{-1}), a mixture of calcite and dolomite (5%), and a mixture of calcite, dolomite (4.75%) and gypsum (0.25%) (Fig. 4). The dissolution of gypsum with at least 8 mmol kg^{-1} of organic matter respiration is needed to explain the highest dissolved Ca values (>3 mmol kg^{-1} (Fig. 5)). We observed excess alkalinity in our samples above model predicted values, while DIC values largely agreed with modeled values (Supplemental Fig. 1). This is potentially due to organic matter contributions to total alkalinity that may be difficult to quantify without further sampling and analyses (Kim et al., 2006; Kim and Lee, 2009). Perry et al. (2002) suggest that shallow root systems in the coastal aquifer may contribute organic matter to the groundwater.

We posit that the dissolved Ca load of terrestrial groundwater is a function of the amount of organic matter respiration that has occurred during transit of the groundwater through the aquifer and the aquifer mineral matrix, resulting in a range of potential pH, alkalinity, DIC and Ca concentrations for the terrestrial end member. With the available data it is not possible to determine the exact combination of organic matter respiration and calcite,

Please cite this article in press as: Gonneea M. E., et al. Trace element geochemistry of groundwater in a karst subterranean estuary (Yucatan Peninsula, Mexico). *Geochim. Cosmochim. Acta* (2014), http://dx.doi.org/10.1016/j.gca.2014.01.037

Table 1
Yucatan aquifer and global average limestone Ba, Sr, U, Mn and Ra isotope concentrations.

Element	μmol g^{-1} or (Ra) dpm g^{-1}	E/Ca (μmol mol^{-1} or (Ra) dpm $mmol^{-1}$)	Location	Reference
Ba	0.17	17	Yucatan	This study
	0.07–0.22	8–30	Yucatan	–[a]
	0.66	66	Global limestone	–[b]
Sr	3.3	330	Yucatan	This study
	2.3–2.6	300–320	Yucatan	–[a]
	2.3–3.3	250–390	Yucatan	–[b]
	7.0	700	Global limestone	–[c]
U	0.0032	0.32	Yucatan	This study
	0.0073–0.0078	0.9–1.1	Yucatan	–[a]
	0.009	0.9	Global limestone	–[b]
Mn	13.1	1310	Yucatan	This study
	38–55	5200–6400	Yucatan	–[a]
	11	1130	Global limestone	–[b]
^{226}Ra	1.5–6.1	0.15–0.61	Yucatan	This study
^{228}Ra	0.17–0.33	0.017–0.033	Yucatan	This study
^{223}Ra	0.02–0.22	0.011–0.035	Yucatan	This study

[a] Tuchscherer et al. (2005).
[b] Bowen (1979).
[c] Schmitt et al. (2004).

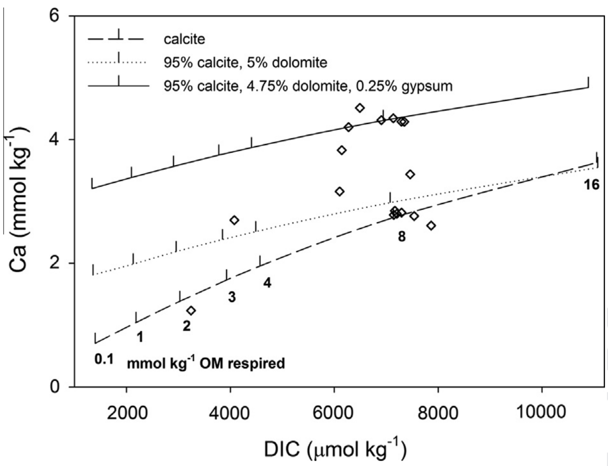

Fig. 4. Ca plotted against DIC for terrestrial (salinity < 2) groundwater samples collected in Dec. 2009 (diamonds). Also shown is the predicted Ca:DIC relationship following organic matter degradation as modeled using PHREEQ (Parkhurst and Appelo, 2013) for equilibrium with 1 mol L^{-1} calcite (dashed line); 95% calcite, 5% dolomite (dotted line) and 95% calcite, 4.75% dolomite and 0.25% gypsum (solid line). Vertical hatch marks and numbers in bold indicate the amount of organic matter respired at each point.

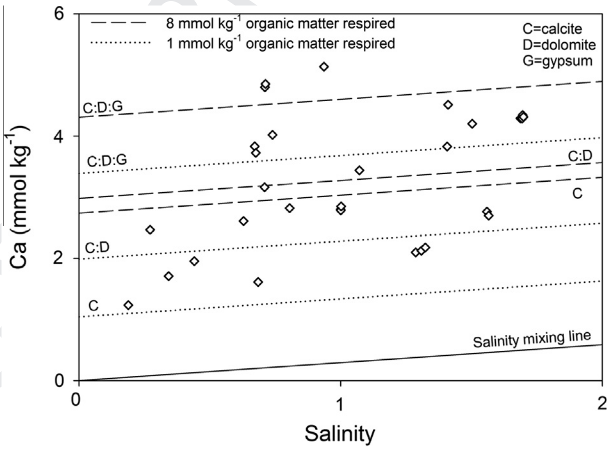

Fig. 5. Predicted terrestrial groundwater dissolved Ca versus salinity following 1 mmol kg^{-1} (dotted lines) and 8 mmol kg^{-1} (dashed lines) organic matter respiration in equilibrium with 1 mol L^{-1} calcite; 95% calcite (C), 5% dolomite (D); and 95% calcite 4.75% dolomite and 0.25% gypsum (G). Addition of dissolved Ca through conservative mixing with ocean waters is shown in the solid line; this contribution has also been added to the mineral equilibrium lines. See Fig. 4 for dissolved Ca in terrestrial groundwater at additional organic matter respiration amounts. All terrestrial (salinity < 2) groundwater samples with measured Ca are shown.

dolomite and gypsum dissolution that has occurred within each terrestrial groundwater sample, rather we use the model results and data to place bounds on the potential for enhanced dissolution and to explain the relatively high groundwater trace element concentrations we report here.

If chemical equilibrium with aquifer minerals, as discussed above, controls the terrestrial groundwater elemental concentrations (i.e. outside of the salinity mixing zone), the relative proportion of the element/calcium ratio (E/Ca) in the aquifer matrix (E/Ca_{solid}) to groundwater ($E/Ca_{groundwater}$) can be predicted from the partition coefficient (K_d):

$$K_d = \frac{E/Ca_{solid}}{E/Ca_{groundwater}} \tag{1}$$

Calcite partition coefficients are readily available to calculate the equilibrium groundwater E/Ca for Ba, Sr, U, Mn and Ra (Table 2). The partition coefficient varies with temperature and environmental conditions (Kitano and

Please cite this article in press as: Gonneea M. E., et al. Trace element geochemistry of groundwater in a karst subterranean estuary (Yucatan Peninsula, Mexico). *Geochim. Cosmochim. Acta* (2014), http://dx.doi.org/10.1016/j.gca.2014.01.037

Table 2
Element radius, calcite partition coefficient and predicted dissolved E/Ca.

Element	Radius[*]	K_d calcite	Predicted dissolved E/Ca (μmol mol^{-1} or dpm mmol^{-1})	K_d Reference
Ba	1.38	0.8	21.25	–[a]
Sr	1.21	0.1	3300	–[b]
U	1.00	0.2	1.6	–[a]
Mn	0.83	50	26.24	–[c]
^{226}Ra	1.48	0.5	0.36–1.2	–[a]
^{228}Ra	1.48	0.5	0.034–0.056	–[a]
^{223}Ra (in equilibrium with ^{227}Ac)	1.48	0.5	0.004–0.044	–[a]
Ca	1.06			

[*] Ionic radii from Shannon (1976).
[a] Rihs et al. (2000).
[b] Kitano and Oomori (1971).
[c] Lorens (1981).

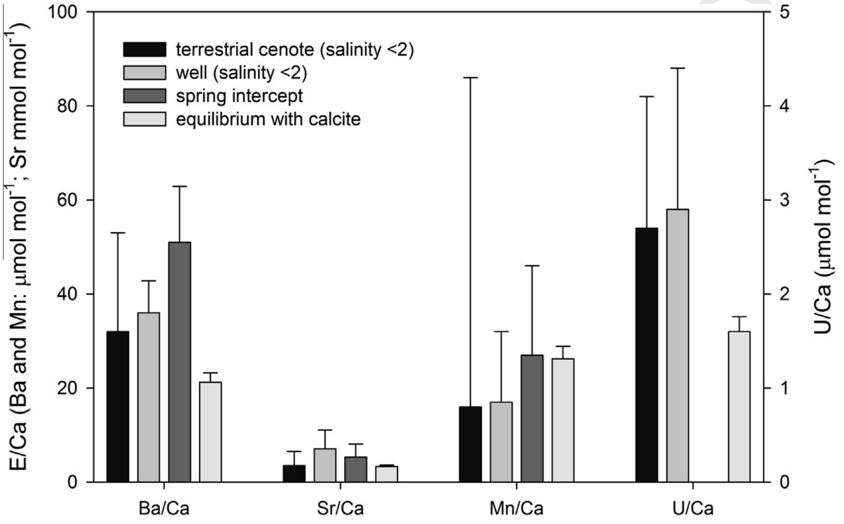

Fig. 6. Ba/Ca, Sr/Ca, Mn/Ca and U/Ca ratios for terrestrial cenote and well (salinity < 2) samples. Also shown is the predicted ratio from the statistically significant spring mixing relationships (i.e. Ba intercept/Ca intercept, Table S3). The groundwater E/Ca ratio in equilibrium with aquifer calcite according to Eq. (1) is also shown. Note separate axis for U/Ca on right.

Oomori, 1971; Lorens, 1981; Rihs et al., 2000). The values used here are based on empirical studies of modern calcite, and may vary for the specific conditions present in the Yucatan aquifer, yet are sufficient to evaluate if the trace element content of terrestrial groundwater results from equilibrium dissolution of aquifer rocks. In addition, the extent to which E/Ca$_{groundwater}$ due to dissolution can be constrained also depends on potential variability in E/Ca$_{solid}$. The available data for the Yucatan (Table 1) suggests the range of E/Ca in the unaltered aquifer matrix is small. Dolomite is a minor mineral in the portion of the aquifer studied here, but may have a different trace element content than calcite (Dawson and Hinton, 2003).The Sr/Ca ratio of the terrestrial end member (2.4 ± 2.6 mmol mol^{-1}) is near that predicted by equilibrium with calcite (3.3 mmol mol^{-1}, Fig. 6 and Table 2). Some well samples have much larger Sr/Ca ratios, coincident with the high Ba/Ca ratios, potentially due to groundwater interactions with aragonite and/or celestite, which have a higher Sr content than calcite. Predicted equilibrium dissolved Ba/Ca is slightly greater than the value observed in the terrestrial groundwater samples (Fig. 6, Table 2). Some well samples (from the east coast) have much higher Ba and ^{228}Ra than expected, potentially due to interaction with aragonite, which has a higher Ba content than calcite. Terrestrial groundwater U/Ca ratios (2.1 ± 1.4 μmol mol^{-1}, Fig. 6) are within error of the predicted value due to chemical equilibrium with calcite (1.6 μmol mol^{-1}, Table 2). Terrestrial groundwater Mn/Ca ratios (16 ± 70 μmol mol^{-1}, Fig. 6) also agree with those predicted by equilibrium with calcite (26 μmol mol^{-1}, Table 2). Terrestrial groundwater ^{226}Ra/Ca, ^{228}Ra/Ca and ^{223}Ra/Ca fall within the predicted ranges (Fig. 7). Terrestrial groundwater trace element and radium concentrations thus appear to largely be explained by dissolution of calcite, the main aquifer mineral, although U is elevated potentially due to complexation with carbonate (see Section 4.3.3). Q4

Please cite this article in press as: Gonneea M. E., et al. Trace element geochemistry of groundwater in a karst subterranean estuary (Yucatan Peninsula, Mexico). *Geochim. Cosmochim. Acta* (2014), http://dx.doi.org/10.1016/j.gca.2014.01.037

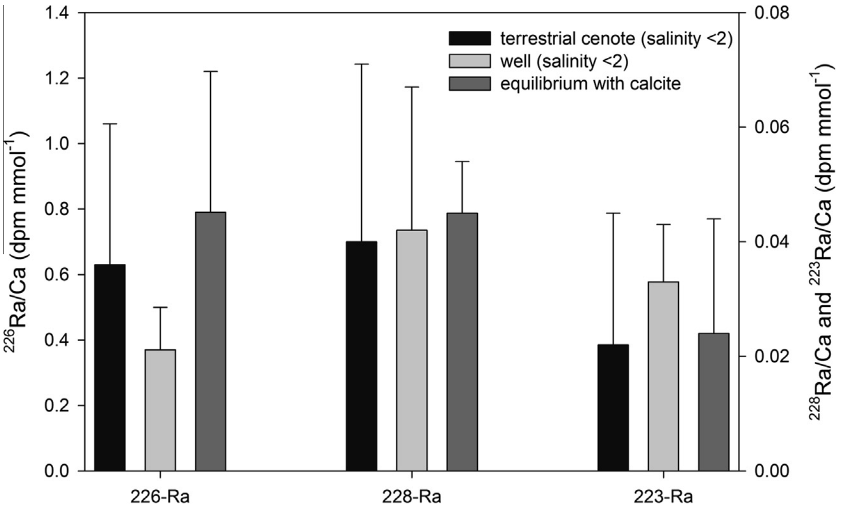

Fig. 7. ^{226}Ra/Ca, ^{228}Ra/Ca and ^{223}Ra/Ca ratios for terrestrial cenote and well samples (salinity < 2) as well as that predicted by rock dissolution according to Eq. (1). Note separate axis for ^{228}Ra/Ca and ^{223}Ra/Ca on right.

4.3. Geochemistry of the karst subterranean estuary mixing zone and marine groundwater

The processes that may modify groundwater geochemistry within the mixing zone include: (1) chemical equilibrium between groundwater and the aquifer matrix as discussed in Section 4.2, (2) conservative mixing between terrestrial and ocean end members, (3) desorption/sorption exchanges with mineral surfaces and (4) *in situ* production and decay for radium isotopes. Mixing between seawater and terrestrial groundwater is predicted to enhance dissolution of the aquifer minerals (Hanshaw and Back, 1980; Stoessell et al., 1989). To determine if mixing induced dissolution was important for the subterranean estuary under study here, we modeled mixing between terrestrial groundwater and the ocean. The calcite saturation index (SI) is calculated according to:

$$SI = \log\left(\frac{a\mathrm{Ca}^{2+}\mathrm{aHCO}_3^-}{a\mathrm{H}^+\mathrm{K}_{\mathrm{calcite}}}\right) \tag{2}$$

where aCa^{2+} refers to the dissolved Ca activity, aHCO$_3^-$ is the carbonate activity and aH$^+$ is pH. K is the equilibrium constant for the formation of calcite (CaCO$_3$) calculated using the temperature-salinity dependence as founding PHREEQ. Even with the limited set of samples from 2009 where carbonate chemistry was determined, we observed a range of possible terrestrial end members. The two groundwater end members with a pH of 7.44 and 8.44, alkalinity of 6890 and 7410 μmol kg^{-1} and 2.8 mmol kg^{-1} Ca did not result in corrosive mixing with seawater, however, a groundwater end member with a pH of 6.95, alkalinity of 6321 μmol kg^{-1} and 3.4 mmol kg^{-1} Ca was corrosive upon mixing (Fig. 8). As discussed previously, such a terrestrial groundwater end member results only after respiration of 16 mmol kg^{-1} of organic matter and equilibration with calcite. There is no evidence for non-conservative addition of Sr, Mn, Ba and U, as might be expected upon mixing induced dissolution, in the spring samples ranging in salinity from 2 to 35. We thus conclude that dissolution may occur during some groundwater mixing, but this phenomenon is not ubiquitous across the Yucatan Peninsula.

4.3.1. *Barium and radium*

Ba serves as a chemical analogue for Ra since they are both group II alkaline earth metals and have comparable ionic radii (Table 3). Similar distributions of barium and long-lived radium isotopes have been observed in subterranean estuaries where conservative mixing dominates (Kiro et al., 2012), where ionic strength dependent desorption occurs (Gonneea et al., 2013) and in carbonate groundwater systems where precipitation/adsorption reactions dominate (Rihs et al., 2000).

Long-lived Ra isotopes are expected to be in secular equilibrium with parent nuclides in marine carbonate deposits of this age (surface outcrops are largely Pliocene, with older rocks deeper in the aquifer (Perry et al., 2009)). The parent nuclide activity is a function of seawater ^{232}Th and ^{238}U at the time of deposition, the calcite partition coefficient for the parent nuclide (Eq. (1)) and any subsequent weathering or alteration that may impact U or Th content. Considering the limited number and large range of Ra/Ca in rock samples measured here, the potential range in aquifer rock Ra/Ca may be even greater. However, the ^{228}Ra:^{226}Ra groundwater activity ratio largely falls within the bounds of the measured rock ratios (Fig. 7).

Spring Ba concentrations fall on a conservative mixing line with a zero salinity intercept of 200 nmol kg^{-1} (dashed line in Fig. 2a), greater than the observed terrestrial end member (122 ± 75 nmol kg^{-1}). Ba peaks at salinity ∼2, the lowest salinity spring sample (Fig. 9). Conversely, there Q5 is no evidence of conservative mixing in spring ^{226}Ra, ^{228}Ra or ^{223}Ra activities, nor is there a clear trend of salinity dependent desorption influencing all spring samples. The observed decoupling between long-lived Ra isotopes and Ba is unusual within the subterranean estuary (Fig. 10).

Please cite this article in press as: Gonneea M. E., et al. Trace element geochemistry of groundwater in a karst subterranean estuary (Yucatan Peninsula, Mexico). *Geochim. Cosmochim. Acta* (2014), http://dx.doi.org/10.1016/j.gca.2014.01.037

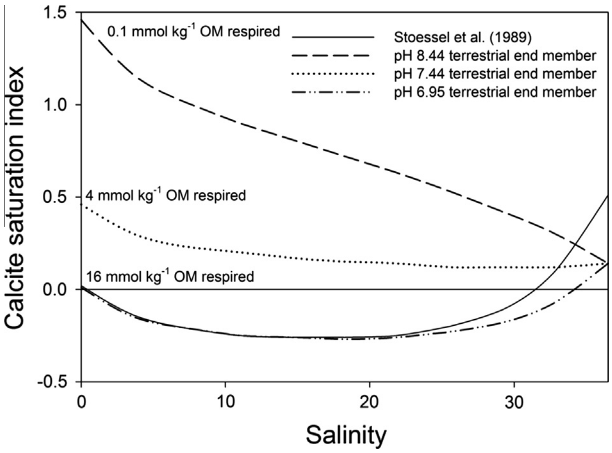

Fig. 8. Predicted calcite saturation index (Eq. (2)) based on mixing between three different terrestrial end members and ocean waters. Mixing between the pH 8.44 and 7.44 (resulting from 0.1 and 4 mmol kg^{-1} organic matter respiration in equilibrium with calcite respectively) and ocean waters does not result in undersaturation (saturation index < 0). However, the pH 6.95 terrestrial end member does produce corrosive waters upon mixing with the ocean. Also shown (solid line) is the mixing relationship predicted by Stoessell et al. (1989) for Yucatan groundwaters. Mixing induced dissolution is therefore a function of the amount of organic matter respired in the terrestrial end member.

Table 3
Radium-tracer based submarine groundwater discharge estimates.

Location	Date	SGD ($m^{-3}\ m^{-1}\ d^{-1}$)	T_w (days)
West coast	Oct-01	50	13
West coast	Jul-02	73 (40)*	7
North coast	May-07	95	12
West coast	May-07	36	14
North coast	Dec-09	84	13
	Average	67 (61)	

* T_w of July 2002 transect is much lower than the other time periods. Value in parentheses indicates SGD if average T_w from all time periods is used rather than 7 days.

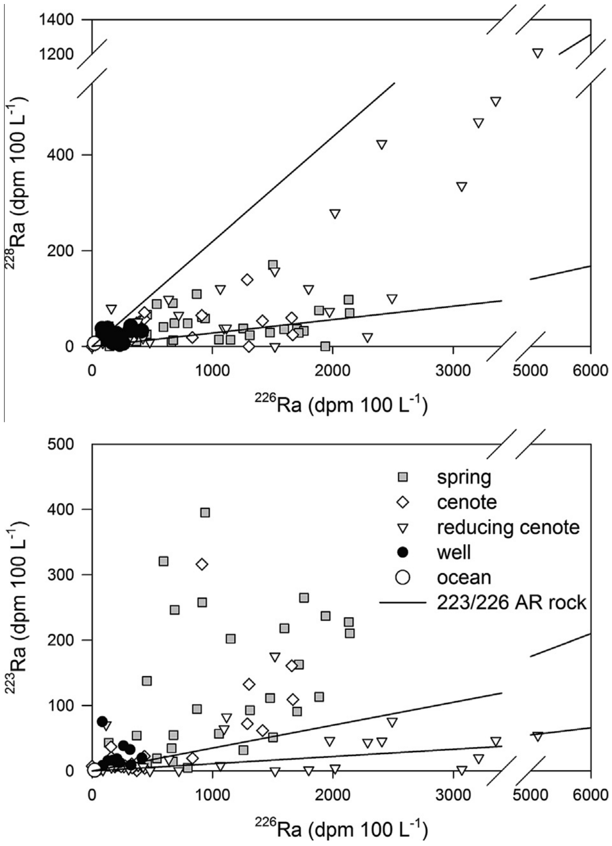

Fig. 9. a) ^{228}Ra:^{226}Ra activity ratios and b) ^{223}Ra:^{226}Ra activity ratios. Solid lines denote the measured aquifer rock activity ratios.

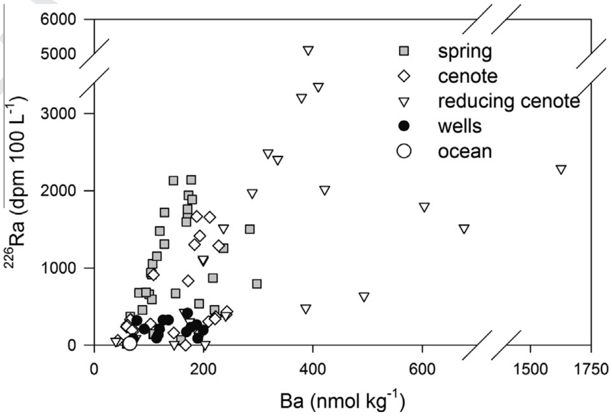

Fig. 10. ^{226}Ra plotted against Ba. The relationship between these elements is somewhat decoupled, particularly in the terrestrial cenote and well samples, potentially due to reduced mobility of the large Ra^{2+} ion compared to Ba^{2+}. There is a linear relationship between a subset of spring (gray squares) and reducing cenote (triangles) samples where conservative mixing of these elements dominates.

One potential explanation is that adsorption of alkaline earth elements increases with ionic radius, thus Ra, with a larger ionic radius than Ba, would be less mobile than Ba (Stumm and Morgan, 1996). Sorption of divalent cations onto calcite has been shown to inhibit movement of dissolved species within aquifers. Under the pH and carbonate ion concentrations present in the Yucatan STE (Stoessell et al., 1989), empirical adsorption coefficients for Ra and Ba predict little change in adsorption across the mixing zone (Zhu, 2002). In addition, there is much greater variability in terrestrial end member ^{226}Ra and ^{228}Ra activities than in Ba concentrations due a greater range in aquifer rock Ra.

Deep cenotes were reducing and anoxic as evidenced by the presence of H_2S in these samples (indicated by strong H_2S smell upon sampling). Perry et al. (2002) suggests that these conditions are due to reduction of terrestrial organic matter that has accumulated in the bottom of cenotes. This organic matter is reduced first using oxygen, then NO_3^-, MnO_2 and finally SO_4^{2-} (Stumm and Morgan, 1996). Ba concentrations in reducing cenotes in excess of that predicted by barite ($BaSO_4$) solubility (modeled saturation in

Please cite this article in press as: Gonneea M. E., et al. Trace element geochemistry of groundwater in a karst subterranean estuary (Yucatan Peninsula, Mexico). Geochim. Cosmochim. Acta (2014), http://dx.doi.org/10.1016/j.gca.2014.01.037

Fig. 2a assumes seawater SO_4^{2-} concentrations) are presumably due to the depletion of SO_4^{2-} in the reducing zone. ^{226}Ra and ^{228}Ra activities are quite high in reducing cenote waters, with a large range in $^{226}Ra/Ca$ and $^{228}Ra/Ca$ ratios (0.01–13 and 0.003–0.703 dpm $mmol^{-1}$ respectively) suggesting that in addition to enhanced aquifer matrix dissolution, Mn-oxide cycling in these reducing environments may maintain elevated Ra activities.

4.3.2. Manganese and uranium

U readily complexes with carbonate, increasing the mobility of uranium in groundwater (Langmuir, 1978). Indeed, terrestrial groundwater U/Ca ratios (2.1 ± 1.4 μmol mol^{-1}, Fig. 6) are higher than predicted by chemical equilibrium with calcite (1.6 μmol mol^{-1}, Table 2). At the high alkalinity (>3 mmol kg^{-1}) and neutral pH values of terrestrial groundwater, dissolved U is largely present as uranyl carbonate complexes, which impede sorption and thus maintain the high U concentrations in terrestrial groundwater and across the spring mixing zone. Under the reducing pH and Eh conditions of the deep cenotes, reduction of uranyl (VI) species to U(IV) results in precipitation of highly insoluble uranium minerals or sorption onto calcite, accounting for the observed removal of U from groundwater (Fig. 2b) (Langmuir, 1978). Likewise, Mn is elevated (100–2600 nmol kg^{-1}) in reducing cenote waters likely due to Mn(IV) reduction.

4.4. Chemical fluxes associated submarine groundwater discharge

Both the water flux and concentration of discharging water must be known to calculate chemical fluxes associated with SGD. We first calculate the radium-tracer based total SGD and compare these values with terrestrial groundwater fluxes derived from recharge-based estimates. We then assign end member concentrations to discharging water and calculate potential trace element fluxes from the Yucatan Peninsula to the coastal ocean. Finally, we explore the potential magnitude of fluxes from karst subterranean estuaries globally and place these estimates in the context of ocean element cycles.

4.4.1. Ra-tracer based SGD estimates

Despite the large variability in Ra activities, these isotopes remain excellent tracers of SGD due to the high concentration gradient between groundwater and seawater. Radium based estimates of SGD were calculated along the west and north coasts of the Yucatan Peninsula in May 2007 and December 2009 (Table 3). In addition, data from offshore radium transects completed in October 2001 and July 2002 were used to extend the temporal and seasonal range of SGD estimates (Young et al., 2008). SGD fluxes are based on coastal ocean radium surveys (Fig. 11). These surveys extend from the coast 3.5–60 km, however the near-shore ^{226}Ra gradient was very steep. In addition, production of ^{223}Ra from shelf sediments (max water depth of 10 m out to 60 km) appears to be large relative to the SGD-derived ^{223}Ra flux over the full transect distance (see Section 4). Thus, we used ^{226}Ra data within 2 km of shore (shaded area in Fig. 11) to calculate the inventory of the long-lived ^{226}Ra according to:

$$^{226}Ra_{SGD} = \frac{[(^{226}Ra_{transect} - {}^{226}Ra_{exchange}) \times V_{transect}]}{T_w} - {}^{226}Ra_{sediment} \quad (3)$$

where $^{226}Ra_{transect}$ is the average activity of the coastal ocean, $^{226}Ra_{exchange}$ is the activity of the water exchanging with this volume, (shelf waters > 2 km: 20 dpm 100 L^{-1}); $V_{transect}$ is the volume of the coastal ocean box; T_w is the average residence time of the water in the box; and $^{226}Ra_{sediment}$ is the sediment flux (Moore, 1996; Charette et al., 2001). Sediment production of ^{226}Ra was calculated assuming ^{230}Th activities in offshore sediments were in secular equilibrium with the sediment ^{226}Ra activity measured in onshore carbonate sands with a partition coefficient of 1 (Beck and Cochran, 2013). $^{226}Ra_{sed}$ fluxes were calculated according to:

$$^{226}Ra_{sediment} = {}^{226}Ra_{rock} \times \rho \times depth \times f_{desorb} \times area \times \lambda_{226} \quad (4)$$

where $^{226}Ra_{rock}$ is the activity of the rock (Table 1), ρ is the density of carbonate sands (2.7 g cm^{-3}), the sediment depth which is flushed with overlying water is 10 cm, the area is shoreline normalized out to 2 km and λ_{226} is the decay constant of ^{226}Ra. Sediment regenerated fluxes are minimal at 30 dpm m^{-1} d^{-1} along a 2 km transect, compared to a $^{226}Ra_{SGD}$ of 10^5–10^6 dpm m^{-1} d^{-1} of shoreline calculated according to Eq. (3). Thus we conclude that SGD is the main source of ^{226}Ra to coastal waters.

We used the short-lived ^{223}Ra to calculate T_w, water residence time, according to:

$$T_w = \frac{\ln\left(\frac{^{223/226}Ra_{transect}}{^{223/226}Ra_{SGD}}\right)}{\lambda_{223}} \quad (5)$$

where $^{223/226}Ra_{transect}$ is the activity ratio of the coastal ocean, $^{223/226}Ra_{SGD}$ is the activity ratio of discharging groundwater (spring average of 0.12) and λ_{223Ra} is the decay constant for ^{223}Ra (Moore, 2000). This model assumes a discrete input at the coast, with mixing and decay controlling the $^{223/226}Ra_{transect}$. An alternative method for calculating residence time is the continuous input model whereby a radium source with a known 223:226 activity ratio is added along the entire transect (Moore et al., 2006). Sediment generated ^{223}Ra inputs likely occur along the shallow Yucatan coast, however, it is unlikely that the 223:226 activity ratio via sediment production will be the same as groundwater discharge, since dissolution and desorption control long-lived concentrations in groundwater, while radioactive decay would be the primary source from coastal sediments. The sediment generated ^{223}Ra flux (calculated according equation 4) is 10^4 dpm m^{-1} d^{-1}, 16–40% of SGD-derived ^{223}Ra flux. This production of ^{223}Ra along the transect is apparent in 223:226 activity ratios that increase with distance from shore (Fig. 11b). Thus, the ages calculated for the Yucatan coast may be an underestimated.

$^{226}Ra_{SGD}$ can be converted from a radium flux to a water flux if the ^{226}Ra activity of groundwater ($^{226}Ra_{GW}$) discharge is known:

Please cite this article in press as: Gonneea M. E., et al. Trace element geochemistry of groundwater in a karst subterranean estuary (Yucatan Peninsula, Mexico). *Geochim. Cosmochim. Acta* (2014), http://dx.doi.org/10.1016/j.gca.2014.01.037

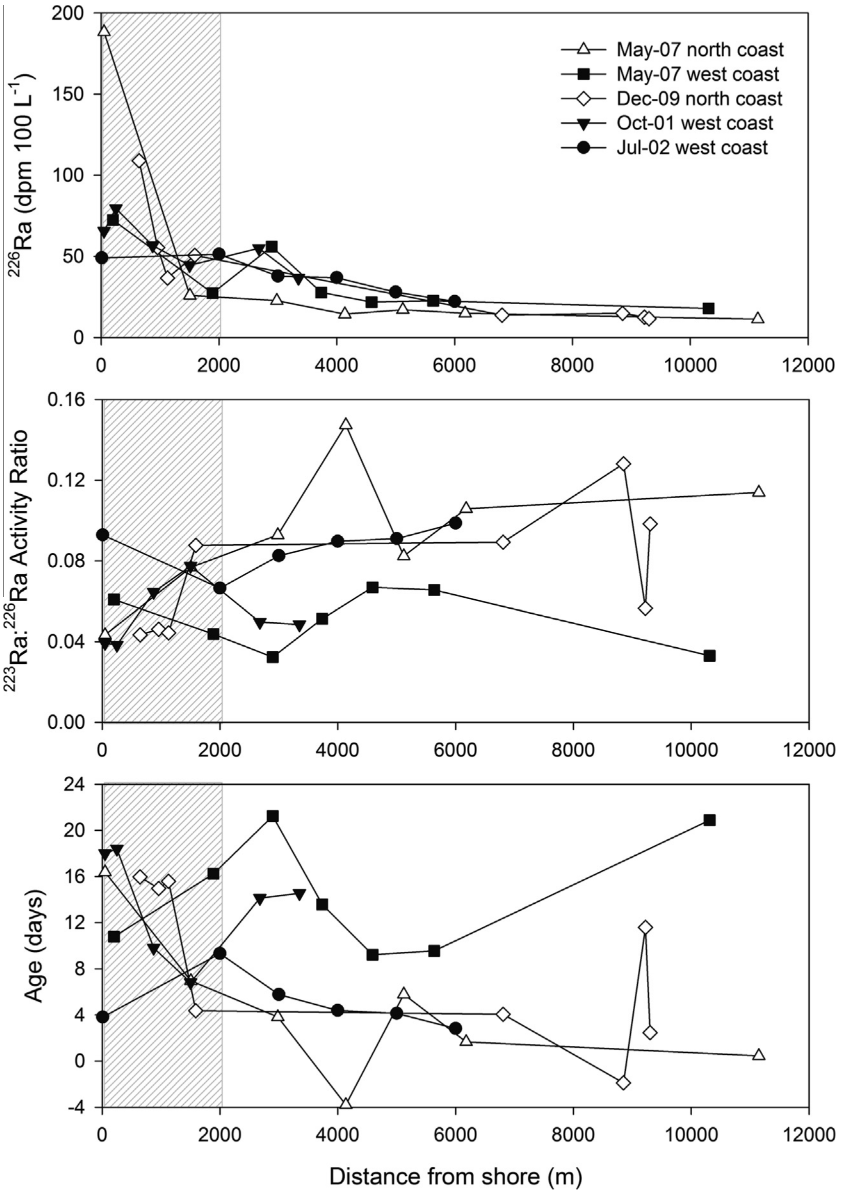

Fig. 11. a) ^{226}Ra activity, b) ^{223}Ra:^{226}Ra activity ratio and c) water age (calculated according to equation (5) for offshore transects in 2001, 2002, 2007 and 2009 along the north and west coast of the Yucatan Peninsula. The shaded area indicates the region used to calculate radium inventories for the tracer-based estimate of submarine groundwater discharge (Table 3).

$$SGD = \frac{^{226}Ra_{SGD}}{^{226}Ra_{GW}} \qquad (6)$$

Here we use the average spring activity for ^{226}Ra$_{GW}$ (1180 ± 490 dpm 100 L^{-1}). Uncertainty is introduced into these estimates primarily from uncertainty in the ^{226}Ra inventory (10%), water ages (30–60%) and in the groundwater end member (40%). Error propagation results in 80–100% uncertainty in total SGD estimates.

Total SGD ranged from 40–95 m^3 m^{-1} d^{-1}. In May 2007 we had measurements along both coasts, and discharge was greater along the North coast (95 m^3 m^{-1} d^{-1}) than the West coast (40 m^3 m^{-1} d^{-1}, Table 3). Here we assume that the sampled springs are representative of submarine groundwater discharge in this region, which may additionally include diffuse discharge away from springs. The salinity of the spring samples used to calculate the Ra end member ranged from 2 to 35, with an average of 9 ± 9, suggesting approximately 75 ± 25% of the discharge was terrestrial, with the remainder due to mixing with marine groundwater. This is in contrast to many other shelf-scale SGD studies where the majority of the SGD is marine in origin (e.g. Moore, 1996; Burnett et al., 2007; Prieto and Destouni, 2011).

The hydrology of the Yucatan Peninsula has been explored in depth through both field studies and modeling approaches (Hanshaw and Back, 1980; Beddows et al., 2007; Gondwe et al., 2010; Bauer-Gottwein et al., 2011). Such studies have assumed that terrestrial discharge was bal-

Please cite this article in press as: Gonneea M. E., et al. Trace element geochemistry of groundwater in a karst subterranean estuary (Yucatan Peninsula, Mexico). *Geochim. Cosmochim. Acta* (2014), http://dx.doi.org/10.1016/j.gca.2014.01.037

anced by net groundwater recharge, which was reported to be 26 $\mathrm{m^3\ m^{-1}\ d^{-1}}$ averaged annually over the 1100 km coastline of the Yucatan Peninsula aquifer (essentially the coastline north of 19°N, Hanshaw and Back, 1980; Gondwe et al., 2010). In all instances the Ra-tracer based discharge shown here is greater than the previously reported terrestrial discharge (Table 3). Patterns of temporal variability in either the marine or terrestrial component of discharge cannot be constrained by the limited number of SGD estimates presented here. Assuming 75% of total discharge is of terrestrial origin, as indicated by spring salinity, we estimate this flux for our study to be 45 ± 20 $\mathrm{m^3\ m^{-1}\ d^{-1}}$.

4.4.2. Yucatan Peninsula trace element fluxes

We extrapolated the spring element concentrations and terrestrial and total SGD estimates across the entire Yucatan coast (1100 km) to calculate trace element fluxes to the ocean. Such an extrapolation is possible for several reasons. First, the conservative mixing behavior observed in actively discharging springs (over a relatively wide spatial scale) for Sr, Ba and Mn and relatively invariant U concentrations simplifies estimates of SGD-derived fluxes since end member concentrations are well constrained. Spring Sr and Mn concentrations lie along a mixing line between terrestrial groundwater in equilibrium with the aquifer rocks and seawater. While spring Ba concentrations are conservative, enrichment at salinity 2 (200 $\mathrm{nmol\ kg^{-1}}$) is observed compared to terrestrial groundwater in chemical equilibrium with aquifer rocks, thus it is the flux of this low salinity spring water that will determine the SGD-associated Ba load. Spring Ra activities display a much larger range and were enriched compared to the terrestrial end member, resulting in a Ra end member that is less well constrained than the other elements. Thus, we conclude that there is minimal alteration of the chemical signature of SGD upon subterranean mixing, except in the case of barium and radium as noted above. Secondly, terrestrial SGD dominates the total SGD flux and is fairly well constrained. We use the water recharge estimate of 26 $\mathrm{m^3\ m^{-1}\ d^{-1}}$ as a minimum flux and the 45 $\mathrm{m^3\ m^{-1}\ d^{-1}}$ reported here as a maximum terrestrial flux. Uncertainty in the marine component of SGD will have minimal impact on the SGD-derived chemical fluxes, especially for Sr, U and Mn. Even for elements where mixed salinity discharge must be considered, the component of marine discharge at salinity 5 (for Ra) and salinity 2 (for Ba) is small.

Submarine groundwater discharge associated Ba fluxes from the Yucatan are 2.3–3.7 × 10^6 $\mathrm{mol\ y^{-1}}$ or 2.1–3.4 $\mathrm{mol\ m^{-1}\ y^{-1}}$ (Table 4). The Ba flux calculated for the Yucatan is only 2–12% of the shoreline normalized flux to the South Atlantic Bight (28–114 $\mathrm{mol\ m^{-1}\ y^{-1}}$, Shaw et al., 1998), but is ~4 times greater than shoreline normalized fluxes reported for a site in the northeast Gulf of Mexico (Santos et al., 2011) and Waquoit Bay, MA (Gonneea et al., 2013). Radium-226 export on the Yucatan Peninsula is 1.5 × 10^{14} $\mathrm{dpm\ y^{-1}}$ (Table 4). This flux (at salinity 5) is within a factor of two of the shoreline normalized fluxes to the South Atlantic Bight (Moore, 1996) and the Mediterranean coast of Spain (Garcia-Solsona et al., 2010), both locations with karst aquifers. In contrast, shoreline normalized ^{226}Ra flux from the sandy aluminosilicate dominated STE of Waquoit Bay is two orders of magnitude less (Gonneea et al., 2013). Sr fluxes calculated for the Yucatan are 2.1–4.0 × 10^8 $\mathrm{mol\ y^{-1}}$ (Table 4), 1–3% of the total global SGD Sr flux (Beck et al., 2013). Yucatan U SGD-associated fluxes are 1.0–2.0 × 10^5 $\mathrm{mol\ y^{-1}}$ (Table 4). U removal

Table 4
Trace element end member and flux from the Yucatan Peninsula.

Element	River EM (nmol $\mathrm{kg^{-1}}$ or Ra dpm 100 $\mathrm{L^{-1}}$)	Karst EM (nmol $\mathrm{kg^{-1}}$ or Ra dpm 100 $\mathrm{L^{-1}}$)	Ratio Karst/River EM	Yucatan karst flux[‡] (mol or Ra dpm $\mathrm{yr^{-1}}$)	River Reference
Ba-salinity 2[*]	168	190[†]	1.2	2.3–3.7 × 10^6	–[a]
Sr	685	20,100	29	2.1–4.0 × 10^8	–[a]
	1208	20,100	17		–[b]
U	1.56	10	6.4	1.0–2.0 × 10^5	–[a]
	2.14		4.7		–[c]
Mn	620	103	0.17	1.1–2.0 × 10^6	–[a]
	127		0.81		–[d]
^{226}Ra-salinity 5[*]	5.3	1000[†]	190	1.7–2.6 × 10^{15}	–[a]
	9.6	1000[†]	96	1.3–2.6 × 10^{15}	–[c]

[*] Ba and Ra concentrations peak at salinities greater than the pure terrestrial groundwater end member. Thus the SGD flux at salinity 2 (for Ba) and 5 (for Ra) is calculated according to: $\mathrm{SGD}_x = \mathrm{SGD}_{\mathrm{terrestrial}} + \mathrm{SGD}_{\mathrm{marine}} \times (\mathrm{salinity}_x/\mathrm{salinity}_{\mathrm{TotalSGD}})$, where x refers to the salinity of interest. $\mathrm{SGD}_{\mathrm{terrestrial}}$ is 26–46 $\mathrm{m^3\ m^{-1}\ d^{-1}}$ (Hanshaw and Back, 1980; Gondwe et al., 2010) and $\mathrm{salinity}_{\mathrm{TotalSGD}}$ is 9.

[†] Karst Ba and ^{226}Ra end members were modified to exclude the component from recirculated marine groundwater. Thus 200 $\mathrm{nmol\ kg^{-1}}$ Ba was reduced to 190 $\mathrm{nmol\ kg^{-1}}$ to account for seawater Ba in the SGD flux at salinity 2, while ^{226}Ra was reduced from 1000 to 996 dpm 100 $\mathrm{L^{-1}}$ at SGD flux at salinity 5.

[‡] Yucatan Peninsula fluxes are calculated for the entire 1,100 km coastline north of 19°N.

[a] Gaillardet et al. (2003).

[b] Peucker-Ehrenbrink et al., 2010.

[c] Chabaux et al., (2003).

[d] Bender et al. (1977).

Please cite this article in press as: Gonneea M. E., et al. Trace element geochemistry of groundwater in a karst subterranean estuary (Yucatan Peninsula, Mexico). *Geochim. Cosmochim. Acta* (2014), http://dx.doi.org/10.1016/j.gca.2014.01.037

occurs within the deep groundwater reaction zone, however, the residence time of this region with regard to coastal ocean exchange is unknown, but appears to be long (Beddows et al., 2007). This removal would result in a lower net flux of U, which cannot be fully constrained in the present study. The Yucatan U flux is ~1% of the global SGD-derived U input of 9.3 ± 8.7 × 10^6 mol y^{-1} proposed by Dunk et al. (2002). Mn fluxes associated with SGD are 1.1–2.0 × 10^6 mol y^{-1}, much less than those reported from a site in Brazil (Sanders et al., 2012), due to the low Mn content of carbonate rock. We did attempt to measure iron in these samples, however our detection limit was 200 nmol kg^{-1} and all but a few of the reducing cenote samples were below this. Thus, it is unlikely that karst subterranean estuaries represent a significant iron flux globally.

4.4.3. Global karst subterranean estuary element fluxes

To evaluate potential global element fluxes associated with submarine groundwater discharge from karst subterranean estuaries, we extrapolate the fluxes for the Yucatan to the 12% of global subterranean estuaries that are karst (Beck et al., 2013). This scaling exercise assumes that: (1) trace element concentrations reported for the Yucatan are representative of those in other karst STEs, (2) there is minimal alteration of the chemical signature of SGD upon subterranean mixing, except as discussed above for Ba and Ra, and (3) discharge of terrestrial (or low salinity) SGD dominates the chemical transport and is of a similar magnitude in other karst settings.

Terrestrial groundwater within carbonate aquifers appears to largely derive its chemical signature from solid-solution equilibrium. Since Yucatan aquifer bedrock trace element content is at the lower range of global limestone values (Bowen, 1979), this may also apply to groundwater trace element concentrations. The terrestrial groundwater flux (26–45 m^3 m^{-1} d^{-1}) is well within the expected range; averaged globally, terrestrial groundwater discharge is 18 m^3 m^{-1} d^{-1} (Zekster et al., 2006). While the discharge of terrestrial groundwater is ultimately linked to inland recharge rates, it is likely that discharge along karstic coastlines is greater than the global average due to the high permeability of these aquifers and typically high precipitation rates. A wide range of terrestrial groundwater discharge rates in karst regions have been reported, from 2 m^3 m^{-1} d^{-1} at one site in Ireland (Einsiedl, 2012) to 120 m^3 m^{-1} d^{-1} along the Spanish coast (Garcia-Solsona et al., 2010). Taken together, these global fluxes represent a reasonable estimate of chemical export from karstic subterranean estuaries. We have not attempted to propagate errors on these estimates, due to limited data on global karst STE end member concentrations and water fluxes.

Submarine groundwater discharge from karst subterranean estuaries is an important source of U, Sr and Ra to the global ocean (Table 5). We found that the Yucatan U end member was 6.4 times greater than the global riverine end member (Table 4, Gaillardet et al. (2003)) making carbonate karst subterranean estuaries potentially an important global source of U (4.0–7.7 × 10^6 mol y^{-1}, 7–33% of river flux, Table 5). Dunk et al. (2002) calculated global SGD-derived U inputs of 9.3 ± 8.7 × 10^6 mol y^{-1}. The global flux we report here is 43–83% of this value, but is derived only from the 12% of the global coastline that is karstic.

The average Sr concentration in Yucatan terrestrial groundwater samples (20.1 μmol kg^{-1}) was 17 times greater than the global riverine end member (1.21 μmol kg^{-1}, Table 4, Peucker-Ehrenbrink et al., 2010) resulting in a Sr flux from karstic subterranean estuaries of 8.2–15.3 × 10^9 mol y^{-1}, ~25% of total river-derived Sr flux (Table 5). This value is within the global meteoric SGD derived Sr flux to the ocean reported by Beck et al. (2013) (7–28 × 10^9 mol y^{-1}). In addition, the global karst SGD Sr flux is about an order of magnitude larger than the SGD derived Sr flux from groundwater discharge in the Ganges–Brahmaputra River system (9 × 10^8 mol y^{-1}) (Basu et al., 2001).

The dominance of groundwater as a source of radium to the ocean has long been recognized (e.g. Moore, 1996; Moore et al., 2008). Here we focus on export of the

Table 5
Global fluxes of elements into the ocean.

Source	Ba (10^9 mol y^{-1})	Sr (10^9 mol y^{-1})	U (10^6 mol y^{-1})	Mn (10^9 mol y^{-1})	^{226}Ra (10^{15} dpm y^{-1})	Reference
River	6.3	29–47	23–59	4.6–23	0.8–2.0	a–j
Hydrothermal		4.3		13.6		k, e, f
Aeolian			1.8	4.2		c, e, f
Weathering/diagenesis		3.4		59.2		k, e, f
Karst groundwater discharge	0.089–0.145	8.2–15.3	4.0–7.7	4.2–7.9	67–99	This study

[a] Gaillardet et al. (2003).
[b] Peucker-Ehrenbrink et al. (2010).
[c] Dunk et al. (2002).
[d] Barnes and Cochran (1990).
[e] Bender et al. (1977).
[f] Martin and Knauer (1980).
[g] Shiller (1997).
[h] Statham et al. (1998).
[i] Moore (1996).
[j] Moore et al. (2008).
[k] Palmer and Edmond (1989).

Please cite this article in press as: Gonneea M. E., et al. Trace element geochemistry of groundwater in a karst subterranean estuary (Yucatan Peninsula, Mexico). *Geochim. Cosmochim. Acta* (2014), http://dx.doi.org/10.1016/j.gca.2014.01.037

longest-lived isotope, ^{226}Ra, since it makes up the majority of the ocean radium inventory. Sparse measurements of riverine dissolved ^{226}Ra activities suggest a median end member of 10 dpm 100 L^{-1} (Chabaux et al., 2003), although Gaillardet et al. (2003) reports a lower value of 5 dpm 100 L^{-1}, resulting in a dissolved river flux of $0.8–2.0 \times 10^{15}$ dpm y^{-1} (Table 5). The karst groundwater end member was averaged across all spring samples (1175 dpm 100 L^{-1}). Given the additional release at salinity 5, the global ^{226}Ra flux from karst STEs is $6.7–9.9 \times 10^{16}$ dpm y^{-1}, 34–126 times the riverine flux (Table 5).

4.5. Conclusions

Groundwater trace element chemistry within the karst Yucatan aquifer is influenced by a variety of processes. Terrestrial groundwater with elevated pCO_2 due to organic matter degradation results in enhanced dissolution of aquifer minerals and elevated dissolved trace element concentrations. Thus, in this setting, the aquifer mineral geochemistry strongly influences groundwater trace element loading. Clearly complimentary analysis of aquifer sediments will enhance studies of subterranean estuary geochemistry in carbonate karst settings. In addition, desorption at low salinity within the mixing zone elevates Ba, ^{226}Ra and ^{228}Ra, while carbonate complexation maintains high U concentrations. Ba, Sr, Ca, and Mn all display conservative mixing in the shallow subterranean estuary typified by coastal springs. Thus there is no evidence of mixing induced dissolution in this portion of the Yucatan STE. Within the deep reducing groundwater, redox processes result in U removal and high Mn concentrations, while Ba, Ca, Sr, ^{226}Ra and ^{228}Ra are elevated due to enhanced dissolution. Submarine groundwater discharge associated transport of U, Mn and Sr may be calculated with a relatively straightforward approach since there is minimal chemical alteration upon mixing within the Yucatan karst STE. Even for Ba, which exhibits a peak at low salinities (2), the terrestrial component of discharge dominates the chemical flux.

Since we do not observe a large enrichment in Ba, Ca, Sr and Ra or depletion of U in spring samples, we conclude that the deep reducing marine groundwater is not actively discharging. Rather, we suggest that the deep anoxic cenote is a groundwater reaction zone that does not take part in shallow subterranean estuary mixing. Additionally, there is no evidence of elevated Sr or depleted U in near shore samples (Charette et al., 2008). Thus, chemical cycling within the regional terrestrial-marine groundwater mixing zone (such as U removal) is not expected to affect large scale SGD associated chemical transport to the coastal ocean. However, it is possible that the deep aquifer dominated by reducing marine groundwater exchanges with the coastal ocean outside the bounds of our study domain (60 km from shore).

Submarine groundwater discharge estimates for the Yucatan Peninsula range from 36 to 95 m^3 m^{-1} d^{-1}, and contained as much as 75 ± 25% terrestrial groundwater, in contrast to many other shelf-scale studies where the recirculated marine component dominates. First order estimates of global fluxes of Sr, U and Ra from karst subterranean estuaries, which only make up 12% of all coastal aquifers, indicate that submarine groundwater discharge fluxes from karst subterranean estuaries are significant contributors to the global ocean budgets of these elements. Recently Beck et al. (2013), presented evidence that SGD is an important source of Sr to the ocean and that isotopic exchange within the subterranean estuary results in groundwater discharge of a more radiogenic end member. Uranium cycling within the subterranean estuary and subsequent discharge via SGD has been posited as both a potential source (Dunk et al., 2002) and sink (Charette and Sholkovitz, 2006; Moore and Shaw, 2008; Santos et al., 2011). There is a need to expand the study of chemical cycling within subterranean estuaries to include a greater diversity of aquifer lithologies and morphologies, as well as mixing regimes, to more fully constrain the potential role SGD plays in global ocean element budgets. For example, relatively little is known about either discharge or chemical cycling within fractured bedrock (Oberdorfer et al., 2008) or volcanic island systems (Peterson et al., 2009; Knee et al., 2010; Povinec et al., 2012), although a substantial amount of groundwater discharge and/or enriched fluid concentrations may result in enhanced chemical fluxes from these types of subterranean estuaries.

ACKNOWLEDGEMENTS

Field assistance was provided by Jessica Fitzsimmons, Alexandra Rao, Simon Richards, Paul Henderson, Crystaline Breier and Dr. Carolina Ruiz Fernandez. Permission to sample groundwater wells was granted by Dr. Arnulk Schiller. Daniel Diamant provided access to his property to sample. Dr. Paul Blanchon and Dr. Roberto Iglesias Prieto provided assistance for work along the east Yucatan coast. DIC and alkalinity measurements were carried out in the laboratories of Dr. Daniel McCorkle and Dr. William Martin at WHOI. Sean Sylva assisted with Ca measurements. M.E.G. was supported by a NDSEG graduate fellowship. Funding for this research was provided by the NSF Chemical Oceanography program (OCE-0751525) and by the Coastal Ocean Institute and the Ocean and Climate Change Institute at Woods Hole Oceanographic Institution. We thank Eugene Perry and one anonymous reviewer for comments on this manuscript.

APPENDIX A. SUPPLEMENTARY DATA

Supplementary data associated with this article can be found, in the online version, at http://dx.doi.org/10.1016/j.gca.2014.01.037.

REFERENCES

ArandaCirerol N., Herrera-Silveira J. A. and Comin F. A. (2006) Nutrient water quality in a tropical coastal zone with groundwater discharge, northwest Yucatan, Mexico. *Estuar. Coast. Shelf Sci.* **68**(3–4), 445–454.

Barnes C. E. and Cochran J. K. (1990) Uranium removal in oceanic sediments and the oceanic-U balance. *Earth Planet. Sci. Lett.* **97**(1–2), 94–101.

Basu A. R., Jacobsen S. B., Poreda R. J., Dowling C. B. and Aggarwal P. K. (2001) Large groundwater strontium flux to the oceans from the bengal basin and the marine strontium isotope record. *Science* **293**(5534), 1470–1473.

Please cite this article in press as: Gonneea M. E., et al. Trace element geochemistry of groundwater in a karst subterranean estuary (Yucatan Peninsula, Mexico). *Geochim. Cosmochim. Acta* (2014), http://dx.doi.org/10.1016/j.gca.2014.01.037

Bauer-Gottwein P. et al. (2011) Review: The Yucatan Peninsula karst aquifer, Mexico. *Hydrogeol. J.* **19**(3), 507–524.

Bautista F., Bautista D. and Delgado-Carranza C. (2009) Calibration of the equations of Hargreaves and Thornthwaite to estimate the potential evapotranspiration in semi-arid and subhumid tropical climates for regional applications. *Atmosfera* **22**(4), 331–348.

Beck A. J., Charette M. A., Cochran J. K., Gonneea M. E. and Peucker-Ehrenbrink B. (2013) Dissolved strontium behavior in the subterranean estuary—implications for the Sr isotope budget of the global ocean. *Geochim. Cosmochim. Acta*. http://dx.doi.org/10.1016/j.gca.2013.03.021.

Beck A. J. and Cochran M. A. (2013) Controls on solid-solution partitioning of radium in saturated marine sands. *Mar. Chem.*. http://dx.doi.org/10.1016/j.marchem.2013.01.008.

Beck A. J. et al. (2007) Importance of geochemical transformations in determining submarine groundwater discharge-derived trace metal and nutrient fluxes. *Appl. Geochem.* **22**(2), 477–490.

Beddows P. A., Smart P. L., Whitaker F. F. and Smith S. L. (2007) Decoupled fresh-saline groundwater circulation of a coastal carbonate aquifer: spatial patterns of temperature and specific electrical conductivity. *J. Hydrol.* **346**(1–2), 18–32.

Bender M. L., Klinkhammer G. P. and Spencer D. W. (1977) Manganese in seawater and the marine manganese balance. *Deep Sea Res.* **24**(9), 799–812.

Bone S. E., Charette M. A., Lamborg C. H. and Gonneea M. E. (2007) Has submarine groundwater discharge been overlooked as a source of mercury to coastal waters? *Environ. Sci. Technol.* **41**(9), 3090–3095.

Boose, E.a.F., D., (2006) Ecological Impacts of Hurricanes Across the Yucatan Peninsula. Harvard Forest Data Archive, HF071, http://harvardforest.fas.harvard.edu.

Bowen H. J. M. (1979) *Environmental Chemistry of the Elements*. Academic Press, London, UK and New York, NY, USA, 333 pp.

Burnett W. C. et al. (2006) Quantifying submarine groundwater discharge in the coastal zone via multiple methods. *Sci. Total Environ.* **367**(2–3), 498–543.

Burnett W. C., Wattayakorn G., Taniguchi M., Dulaiova H., Sojisuporn P., Rungsupa S. and Ishitobi T. (2007) Groundwater-derived nutrient inputs to the Upper Gulf of Thailand. *Cont. Shelf Res.* **27**, 176–190.

Cervantes-Martinez A., Elias-Gutieerrez M. and Suarez-Morales E. (2002) Limnological and morphometrical data of eight karstic systems 'cenotes' of the Yucatan Peninsula, Mexico, during the dry season (February–May, 2001). *Hydrobiologia* **482**(1–3), 167–177.

Chabaux F., Riotte J. and Dequincey O. (2003) U–Th–Ra fractionation during weathering and river transport. *Rev. Mineral. Geochem. Uranium-Series Geochem.*, 533–576.

Charette M. A., Buesseler K. O. and Andrews J. E. (2001) Utility of radium isotopes for evaluating the input and transport of groundwater-derived nitrogen to a Cape Cod estuary. *Limnol. Oceanogr.* **46**(2), 465–470.

Charette M. A., Gonneea M. E., Henderson P. B., Rao A. and Herrera-Silveira J. (2008) *Trace metal biogeochemistry in karstic subterranean estuaries*. AGU/ASLO Ocean Sciences Meeting, Orlando, Florida.

Charette M. A. and Sholkovitz E. R. (2006) Trace element cycling in a subterranean estuary: Part 2. Geochemistry of the pore water. *Geochim. Cosmochim. Acta* **70**(4), 811–826.

Dawson J. B. and Hinton R. W. (2003) Trace-element content and partitioning in calcite, dolomite and apatite in carbonatite, Phalaborwa, South Africa. *Mineral. Mag.* **67**, 921–930.

Dunk R. M., Mills R. A. and Jenkins W. J. (2002) A reevaluation of the oceanic uranium budget for the Holocene. *Chem. Geol.* **190**(1–4), 45–67.

Einsiedl F. (2012) Sea-water/groundwater interactions along a small catchment of the European Atlantic coast. *Appl. Geochem.* **27**(1), 73–80.

Escobar-Sanchez J. E. and Urrutia-Fucugauchi J. (2010) Chicxulub crater post-impact hydrothermal activity – evidence from Paleocene carbonates in the Santa Elena borehole. *Geofisica Internacional* **49**(2), 97–106.

Fleury P., Bakalowicz M. and de Marsily G. (2007) Submarine springs and coastal karst aquifers: a review. *J. Hydrol.* **339**(1–2), 79–92.

Gaillardet J., Viers J. and Dupre B. (2003) 5.09 – trace elements in river waters. In *Treatise on Geochemistry* (eds. D. H. Heinrich and K. T. Karl). Pergamon, Oxford, pp. 225–272.

Garcia-Solsona E. et al. (2010) Groundwater and nutrient discharge through karstic coastal springs (Castello, Spain). *Biogeosciences* **7**(9), 2625–2638.

Gibbs M. T. and Kump L. R. (1994) Global chemical erosion during the last glacial maximum and the present-sensitivity to changes in lithology and hydrology. *Paleoceanography* **9**(4), 529–543.

Giddings L. and Soto M. (2003) Rhythms of Precipitation in the Yucatan Peninsula. In *The Lowland Maya Area: Three Millennia at the Human–Wildland Interface* (eds. A. Gomez-Pompa, M. F. Allen, S. L. Fedick and J. J. Jimene-Osornio). Food Products Press, p. 659.

Giffin C., Kaufman A. and Broecker W. (1963) Delayed coincidence counter for the assay of actinon and thoron. *J. Geophys. Res.* **68**(6), 1749–1757.

Gondwe B. R. N. et al. (2010) Hydrogeology of the south-eastern Yucatan Peninsula: New insights from water level measurements, geochemistry, geophysics and remote sensing. *J. Hydrol.* **389**(1–2), 1–17.

Gonneea M. E., Morris P. J., Dulaiova H. and Charette M. A. (2008) New perspectives on radium behavior within a subterranean estuary. *Mar. Chem.* **109**(3–4), 250–267.

Gonneea M. E., Mulligan A. and Charette M. A. (2013) Seasonal cycles in radium and barium within a subterranean estuary: implications for groundwater derived chemical fluxes to surface waters. *Geochim. Cosmochim. Acta*. http://dx.doi.org/10.1016/j.gca.2013.05.034.

Griffith E. M., Paytan A., Caldeira K., Bullen T. D. and Thomas E. (2008) A dynamic marine calcium cycle during the past 28 million years. *Science* **322**(5908), 1671–1674.

Hanshaw B. B. and Back W. (1980) Chemical mass-wasting of the norhtern Yucatan Peninsula by groundwater dissolution. *Geology* **8**(5), 222–224.

Herrera-Silveira J. A., Medina-Gomez I. and Colli R. (2002) Trophic status based on nutrient concentration scales and primary producers community of tropical coastal lagoons influenced by groundwater discharges. *Hydrobiologia* **475**(1), 91–98.

Hess J., Bender M. L. and Schilling J. G. (1986) Evolution of the ratio of Sr-87 to Sr-86 in seawater from Cretaceous to present. *Science* **231**(4741), 979–984.

Holmden C., Papanastassiou D. A., Blanchon P. and Evans S. (2012) Delta Ca-44/40 variability in shallow water carbonates and the impact of submarine groundwater discharge on Ca-cycling in marine environments. *Geochim. Cosmochim. Acta* **83**, 179–194.

Kaleris V. (2006) Submarine groundwater discharge: effects of hydrogeology and of near shore surface water bodies. *J. Hydrol.* **325**(1–4), 96–117.

Please cite this article in press as: Gonneea M. E., et al. Trace element geochemistry of groundwater in a karst subterranean estuary (Yucatan Peninsula, Mexico). *Geochim. Cosmochim. Acta* (2014), http://dx.doi.org/10.1016/j.gca.2014.01.037

Kim H., Lee K. and Choi W. (2006) Contribution of phytoplankton and bacterial cells to the measured alkalinity of seawater. *Limnol. Oceanogr.* **51**(1), 331–338.

Kim H. and Lee K. (2009) Significant contribution of dissolved organic matter to seawater alkalinity. *Geophys. Res. Lett.*. http://dx.doi.org/10.1029/2009GL040271.

Kiro Y., Yechieli Y., Voss C. I., Starinsky A. and Weinstein Y. (2012) Modeling radium distribution in coastal aquifers during sea level changes: the Dead Sea case. *Geochim. Cosmochim. Acta* **88**, 237–254.

Kitano Y. and Oomori T. (1971) The coprecipitation of uranium with calcium carbonate. *J. Oceanogr. Soc. Japan* **27**, 34–42.

Knee K. L., Street J. H., Grossman E. E., Boehm A. B. and Paytan A. (2010) Nutrient inputs to the coastal ocean from submarine groundwater discharge in a groundwater-dominated system: Relation to land use (Kona coast, Hawaii, USA). *Limnol. Oceanogr.* **55**(3), 1105–1122.

Langmuir D. (1978) Uranium solution-mineral equilibria at low-temperatures with applications to sedimentary ore-deposits. *Geochim. Cosmochim. Acta* **42**(6), 547–569.

Langmuir D. and Riese A. C. (1985) The thermodynamic properties of radium. *Geochim. Cosmochim. Acta* **49**(7), 1593–1601.

Lorens R. B. (1981) Sr, Cd, Mn and Co distribution coefficients in calcite as a functino of calcite precipitation rate. *Geochim. Cosmochim. Acta* **45**(4), 553–561.

Martin J. H. and Knauer G. A. (1980) Manganese cycling in Northeast Pacific waters. *Earth Planet. Sci. Lett.* **51**(2), 266–274.

Moore W. S. (1996) Large groundwater inputs to coastal waters revealed by Ra-226 enrichments. *Nature* **380**(6575), 612–614.

Moore W. S. (1999) The subterranean estuary: a reaction zone of ground water and sea water. *Mar. Chem.* **65**(1–2), 111–125.

Moore W. S. (2000) Determining coastal mixing rates using radium isotopes. *Cont. Shelf Res.* **20**(15), 1993–2007.

Moore W. S. (2010) The effect of submarine groundwater discharge on the ocean. *Ann. Rev. Mar. Sci.* **2**, 59–88.

Moore W. S. and Arnold R. (1996) Measurement of Ra-223 and Ra-224 in coastal waters using a delayed coincidence counter. *J. Geophys. Res. Oceans* **101**(C1), 1321–1329.

Moore W. S., Blanton J. O. and Joye S. B. (2006) Estimates of flushing times, submarine groundwater discharge, and nutrient fluxes to Okatee Estuary, South Carolina. *J. Geophys. Res. Oceans* **111**(C9).

Moore W. S. and Reid D. F. (1973) Extraction of Radium from Natural Waters Using Manganese-Impregnated Acrylic Fibers. *J. Geophys. Res.* **78**(36), 8880–8886.

Moore W. S., Sarmiento J. L. and Key R. M. (2008) Submarine groundwater discharge revealed by Ra-228 distribution in the upper Atlantic Ocean. *Nat. Geosci.* **1**(5), 309–311.

Moore W. S. and Shaw T. J. (2008) Fluxes and behavior of radium isotopes, barium, and uranium in seven Southeastern US rivers and estuaries. *Mar. Chem.* **108**(3–4), 236–254.

Morales-Ojeda S. M., Herrera-Silveira J. A. and Montero J. (2010) Terrestrial and oceanic influence on spatial hydrochemistry and trophic status in subtropical marine near-shore waters. *Water Res.* **44**(20), 5949–5964.

Oberdorfer J. A., Charette M., Allen M., Martin J. B. and Cable J. E. (2008) Hydrogeology and geochemistry of near-shore submarine groundwater discharge at Flamengo Bay, Ubatuba, Brazil. *Estuar. Coast. Shelf Sci.* **76**(3), 457–465.

Palmer M. R. and Edmond J. M. (1989) The strontium isotope budget of the modern ocean. *Earth Planet. Sci. Lett.* **92**(1), 11–26.

Parkhurst, D.L. and Appelo, C.A.J., 2013. Description of input and examples for PHREEQC version 3—A computer program for speciation, batch-reaction, one-dimensional transport, and inverse geochemical calculations: U.S. Geological Survey Techniques and Methods, book 6, chap. A43. available only at http://pubs.usgs.gov/tm/06/a43/, 497 pp.

Paytan A., Kastner M. and Chavez F. P. (1996) Glacial to interglacial fluctuations in productivity in the equatorial Pacific as indicated by marine barite. *Science* **274**(5291), 1355–1357.

Perry E., Marin L., McClain J. and Velazquez G. (1995) Ring of cenotes (sinkholes), northwest Yucatan, Mexico – its hydrogeologic characteristics and possible association with the Chicxulub impact crater. *Geology* **23**(1), 17–20.

Perry E., Paytan A., Pedersen B. and Velazquez-Oliman G. (2009) Groundwater geochemistry of the Yucatan Peninsula, Mexico: constraints on stratigraphy and hydrogeology. *J. Hydrol.* **367**(1–2), 27–40.

Perry E., Velazquez-Oliman G. and Marin L. (2002) The hydrogeochemistry of the karst aquifer system of the northern Yucatan Peninsula, Mexico. *Int. Geol. Rev.* **44**(3), 191–221.

Peterson R. N., Burnett W. C., Glenn C. R. and Johnson A. G. (2009) Quantification of point-source groundwater discharges to the ocean from the shoreline of the Big Island, Hawaii. *Limnol. Oceanogr.* **54**(3), 890–904.

Peucker-Ehrenbrink B., Miller M. W., Arsouze T. and Jeandel C. (2010) Continental bedrock and riverine fluxes of strontium and neodymium isotopes to the oceans. *Geochem. Geophys. Geosyst.* **11**, 10–15.

Prieto C. and Destouni G. (2011) Is submarine groundwater discharge predictable? *Geophys. Res. Lett*. http://dx.doi.org/10.1029/2010GL045621.

Povinec P. P. et al. (2012) Isotopic, geophysical and biogeochemical investigation of submarine groundwater discharge: IAEA-UNESCO intercomparison exercise at Mauritius Island. *J. Environ. Radioact.* **103**(2), 24–45.

Price R. M., Savabi M. R., Jolicoeur J. L. and Roy S. (2010) Adsorption and desorption of phosphate on limestone in experiments simulating seawater intrusion. *Appl. Geochem.* **25**(7), 1085–1091.

Reeve A. S. and Perry E. C. (1994) Carbonate geochemistry and the concentrations of aqueous Mg^{2+}, Sr^{2+} and Ca^{2+} – Western North coast of the Yucatan, Mexico. *Chem. Geol.* **112**(1–2), 105–117.

Rihs S., Condomines M. and Sigmarsson O. (2000) U, Ra and Ba incorporation during precipitation of hydrothermal carbonates: Implications for Ra-226-Ba dating of impure travertines. *Geochim. Cosmochim. Acta* **64**(4), 661–671.

Rushdi A. I., McManus J. and Collier R. W. (2000) Marine barite and celestite saturation in seawater. *Mar. Chem.* **69**(1–2), 19–31.

Sanders C. J., Santos I. R., Barcellos R. and Silva E. V. (2012) Elevated concentrations of dissolved Ba, Fe and Mn in a mangrove subterranean estuary: consequence of sea level rise? *Cont. Shelf Res.* **43**, 86–94.

Santos I. R. et al. (2011) Uranium and barium cycling in a salt wedge subterranean estuary: the influence of tidal pumping. *Chem. Geol.* **287**(1–2), 114–123.

Schmitt R. T., Wittmann A. and Stoffler D. (2004) Geochemistry of drill core samples from Yaxcopoil-1, Chicxulub impact crater, Mexico. *Meteorit. Planet. Sci.* **39**(6), 979–1001.

Schmitter-Soto J. J. et al. (2002) Hydrogeochemical and biological characteristics of cenotes in the Yucatan Peninsula (SE Mexico). *Hydrobiologia* **467**(1–3), 215–228.

Shaw T. J., Moore W. S., Kloepfer J. and Sochaski M. A. (1998) The flux of barium to the coastal waters of the southeastern USA: The importance of submarine groundwater discharge. *Geochim. Cosmochim. Acta* **62**(18), 3047–3054.

Shiller A. M. (1997) Manganese in surface waters of the Atlantic Ocean. *Geophys. Res. Lett.* **24**(12), 1495–1498.

Please cite this article in press as: Gonneea M. E., et al. Trace element geochemistry of groundwater in a karst subterranean estuary (Yucatan Peninsula, Mexico). *Geochim. Cosmochim. Acta* (2014), http://dx.doi.org/10.1016/j.gca.2014.01.037

Smith, S.V., Crossland, J.I.M., Crossland, C.J., 1999. Land-Ocean Interactions in the Coastal Zone (LOICZ): Mexican and Central American Coastal Lagoon Systems: Carbon, Nitrogen and Phosphorous Fluxes (Regional Workshop II).

Statham P. J., Yeats P. A. and Landing W. M. (1998) Manganese in the eastern Atlantic Ocean: processes influencing deep and surface water distributions. *Mar. Chem.* **61**(1–2), 55–68.

Stoessell R. K., Moore Y. H. and Coke J. G. (1993) The occurrence and effect of sulfate reduction and sulfide oxidation on coastal limestone dissolution in Yucatan cenotes. *Ground Water* **31**(4), 566–575.

Stoessell R. K., Ward W. C., Ford B. H. and Schuffert J. D. (1989) Water chemistry and CaCO3 dissolution in the saline part of an open-flow mixing zone, coastal Yucatan Peninsula, Mexico. *Geol. Soc. Am. Bull.* **101**(2), 159–169.

Stumm W. and Morgan J. J. (1996) *Aquatic Chemistry*. John Wiley & Sons Inc, 1022 pp..

Torres-Talamante O., Alcocer J., Beddows P. A., Escobar-Briones E. G. and Lugo A. (2011) The key role of the chemolimnion in meromictic cenotes of the Yucatan Peninsula, Mexico. *Hydrobiologia* **677**(1), 107–127.

Tribovillard N., Algeo T. J., Lyons T. and Riboulleau A. (2006) Trace metals as paleoredox and paleoproductivity proxies: an update. *Chem. Geol.* **232**(1–2), 12–32.

Tuchscherer M. G., Reimold W. U., Koeberl C. and Gibson R. L. (2005) Geochemical and petrographic characteristics of impactites and Cretaceous target rocks from the Yaxcopoil-1 borehole, Chicxulub impact structure, Mexico: Implications for target composition. *Meteorit. Planet. Sci.* **40**(9–10), 1513–1536.

Young M. B. et al. (2008) Characterizing sources of groundwater to a tropical coastal lagoon in a karstic area using radium isotopes and water chemistry. *Mar. Chem.* **109**(3–4), 377–394.

Zekster I. S., Everett L. G. and Dzhamalov R. G. (2006) *Submarine Groundwater*. CRC Press, 466 pp..

Zhu C. (2002) Estimation of surface precipitation constants for sorption of divalent metals onto hydrous ferric oxide and calcite. *Chem. Geol.* **188**(1–2), 23–32.

Associate editor: Marc Norman

Please cite this article in press as: Gonneea M. E., et al. Trace element geochemistry of groundwater in a karst subterranean estuary (Yucatan Peninsula, Mexico). *Geochim. Cosmochim. Acta* (2014), http://dx.doi.org/10.1016/j.gca.2014.01.037